Normal Diffusion Tensor Imaging-Based White Matter Anatomy

12

Bram Stieltjes

Learning Points

- Normal diffusion tensor imaging-based anatomy of the healthy brain.
- The identification of several major white matter fiber bundles on 2D directionally encoded color fractional anisotropy maps in axial, coronal, and sagittal views.
- The identification of common 3D virtual reconstructions of DTI-based white matter fiber tracts.
- Region-of-interest placement in order to virtually reconstruct commonly identified DTI-based white matter fiber tracts.

B. Stieltjes, MD, PhD (✉)
Department of radiology and nuclear medicine,
University Hospital Basel,
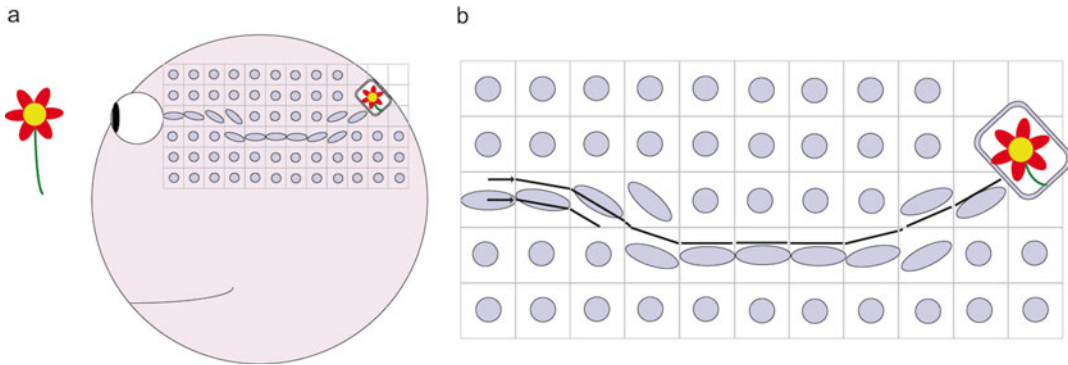Basel, Switzerland
e-mail: B.Stieltjes@dkfz-heidelberg.de

Representation of White Matter Anatomy Using Diffusion Tensor Imaging

As diffusion tensor imaging permits estimation of the main nerve fiber direction within a voxel, a natural extension is to reconstruct the course of whole nerve tracts [1–7]. Figure 12.1 shows a sketch of a brain with diffusion tensor ellipsoids plotted in several brain voxels. The considered person is watching a red-leaved flower. This information is caught by the eye and passed to the visual brain cortex through the optical tract. This tract is observable in the tensor ellipsoids: they are elongated in tract voxels and reflect the main fiber direction. In the sketch, the diffusion is isotropic in voxels not containing the optic tract.

Figure 12.1b illustrates a straightforward approach to reconstruct tracts from the tensor ellipsoids, the so-called FACT algorithm (FACT=fiber assignment by continuous tracking) [4, 5]. The tract is started in one voxel and it follows the orientation of the ellipsoid in this voxel until it hits the border of the voxel. Then, this process is iterated in the adjacent voxel. Usually several starting points—which are also called seeds—are chosen. For example, in

Fig. 12.1 The principle of fiber tracking. (**a**) Schematic view of a person watching a flower. Information is transported from the eye to the visual cortex at the back of the head. (**b**) Close-up of the voxel-wise diffusion measure-ment. The optical tract shows anisotropic (ellipsoid) water displacement and the tract can be reconstructed using dif-fusion tensor imaging

Fig. 12.1b, the tract starting in the center of the initial voxel does not reach the end of the optic nerve tract, since the tract is interrupted when it reaches a voxel with isotropic diffusion. The other tract, which starts in the upper part of the initial voxel, reaches the visual brain cortex. Thus, by choosing several seeds instead of only one seed, the chance is increased that the actual tract is reconstructed.

In Fig. 12.1b, an important property of fiber tracking results can be appreciated: the strong dependency on the chosen algorithm and its parameters. The termination criterion of the algorithm depicted in Fig. 12.1b is to stop the tract if an isotropic voxel is reached. However, if the tract were allowed to maintain its direc-tion in an isotropic voxel under the condition that the next voxel is anisotropic, then the broken fiber would make it to the end of the optic tract. In practice, of course, voxels are usually not perfectly isotropic, so one would rather choose a certain anisotropy threshold to terminate the fiber. The final tracking result will in any case depend strongly on this threshold. As there is often no unique and perfect choice of algorithm and parameters, the obtained results should not be regarded as a perfect

ground truth. Nonetheless, it has been shown that the main fiber tracts can be reconstructed correctly.

Since the initial works on fiber tracking, many fiber tracking algorithms and strategies have been developed. Since a detailed review of these techniques is beyond the scope of this introduction and covered in Chap. 11 of this book, here we only present an in-depth descrip-tion of the algorithm used for the fiber tracking in the "Three-Dimensional Tract Representation" section.

Protocol

Data Acquisition

The data were acquired using a 3 T scanner (TIM Trio, Siemens, Erlangen, Germany) equipped with a 32-channel head coil. A single-shot echo-planar imaging (EPI) sequence was applied for DTI assessment (TR 6400 ms, TE 91 ms, 96×96 matrix size, field of view 240 mm). Fifty axial slices with a thickness of 2.5 mm and no gap, 60 gradient directions, and two b-values (0 and 1000 s/mm^2) were obtained.

Data Preprocessing

Eddy currents and head motion were corrected using *FSL flirt* (www.fmrib.ox.ac.uk/fsl/) by affine registration of the baseline and diffusion weighted volumes to the first baseline volume. Gradient directions were corrected according to the transformation. FSL bet was used in order to estimate brain masks. Tensors were fit using the teem library (teem.sourceforge.net). Negative Eigenvalues were corrected by adding (to all Eigenvalues) the amount by which the smallest is negative (corresponding to increasing the non-diffusion weighted image value).

Tracking Algorithm

The tractography algorithm that was used to generate the fiber tracking results was originally introduced by Reisert et al. [8] and is a so-called global tracking algorithm [9, 10]. This algorithm ranked first in an evaluation study by Fillard et.al. on the performance of tractography algorithms [11] and is implemented in MITK-Diffusion ([12], www.mitk.org/Difusion). The complete procedure is described in more detail in [13].

Two-Dimensional Tract Representation

Introduction (2D)

Here we present a diffusion tensor imaging derived color map produced using MITK-Diffusion ([12], www.mitk.org/Difusion). In these maps, the directional orientation of fiber tracts is color coded in the following fashion: tracts moving left-right are coded red (e.g., the Corpus callosum), anterior-posterior tracts are coded green (e.g., the Cingulum), and cranio-caudal tracts are coded blue (e.g., the cortico-spinal tract). The intensity or hue indicates the fractional anisotropy, a measure of fiber density.

The most important, central parts of the brain are displayed in the three main radiological planes, axial, coronal, and sagittal.

Two-Dimensional Anatomy

Axial slices (Figs. 12.2, 12.3, 12.4, 12.5, 12.6, 12.7, 12.8, 12.9, and 12.10)

   Coronal slices (Figs. 12.11, 12.12, 12.13, 12.14, 12.15, 12.16, 12.17, 12.18, and 12.19)

   Sagittal slices (Figs. 12.20, 12.21, 12.22, 12.23, 12.24, 12.25, 12.26, and 12.27)

Three-Dimensional Tract Representation

Introduction (3D)

The three-dimensional part covers the most prominent white matter connections within the cerebral hemispheres. The complete reconstruction process is covered in a consistent, step-by-step fashion. First the relevance and anatomy of the tract is discussed and an initial region of interest (ROI) is shown. This ROI is chosen as to yield an optimal final result. By using inclusion (green) and exclusion (red) ROIs, the result is further refined. The final result is represented without the ROIs to optimally appreciate the anatomical location. The color coding of these tracts is identical to the two-dimensional color maps (section, Introduction 2D). The intricate anatomy of important adjacent tracts is further illustrated in combined overviews. Here each individual tract is represented in unicolor to enhance the visualization of the complex, inter-woven anatomy.

Three-Dimensional Anatomy

The Corpus Callosum
Fiber tracking of the corpus callosum is relatively straightforward. Select a midsagittal on the sagit-
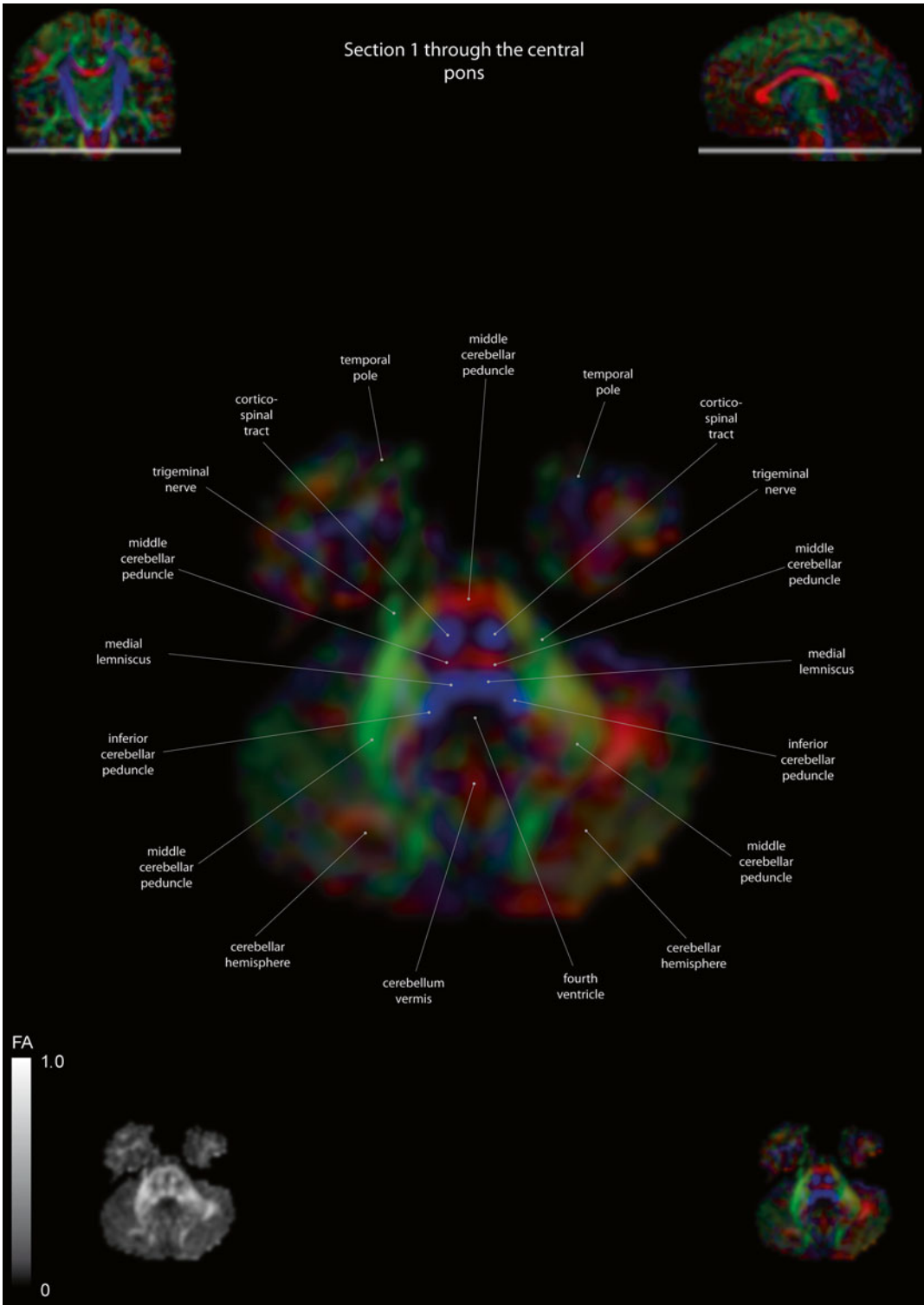
Fig. 12.2 Axial slices of a color-coded diffusion tensor image. The colors represent fiber direction; *red* = left to right, *blue* = cranio-caudal, and *green* = anterior-posterior. The intensity represents the fractional anisotropy (FA) also indicated in the *lower corner*. In the *upper corners*, the slice section is indicated in the coronal and sagittal plane
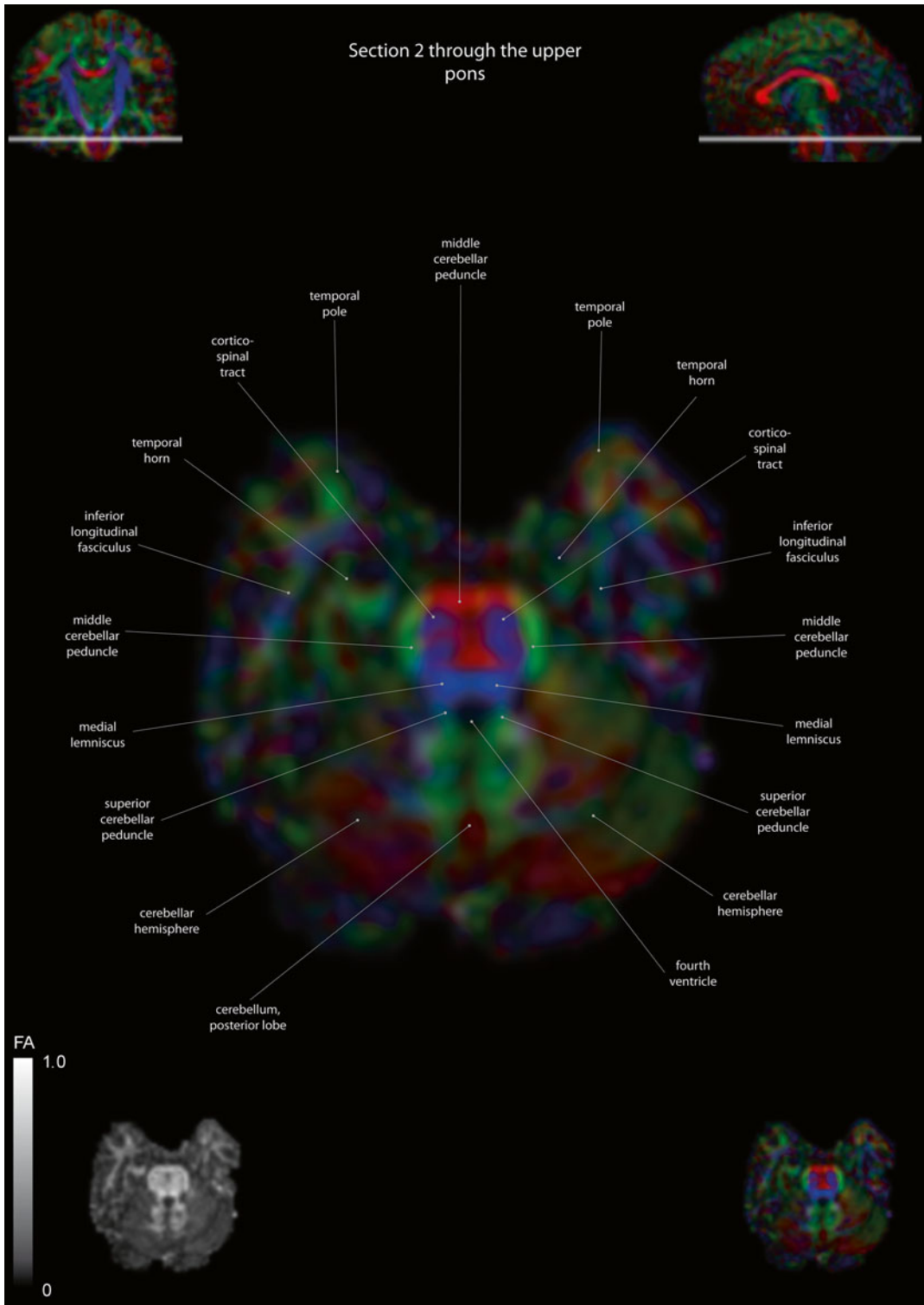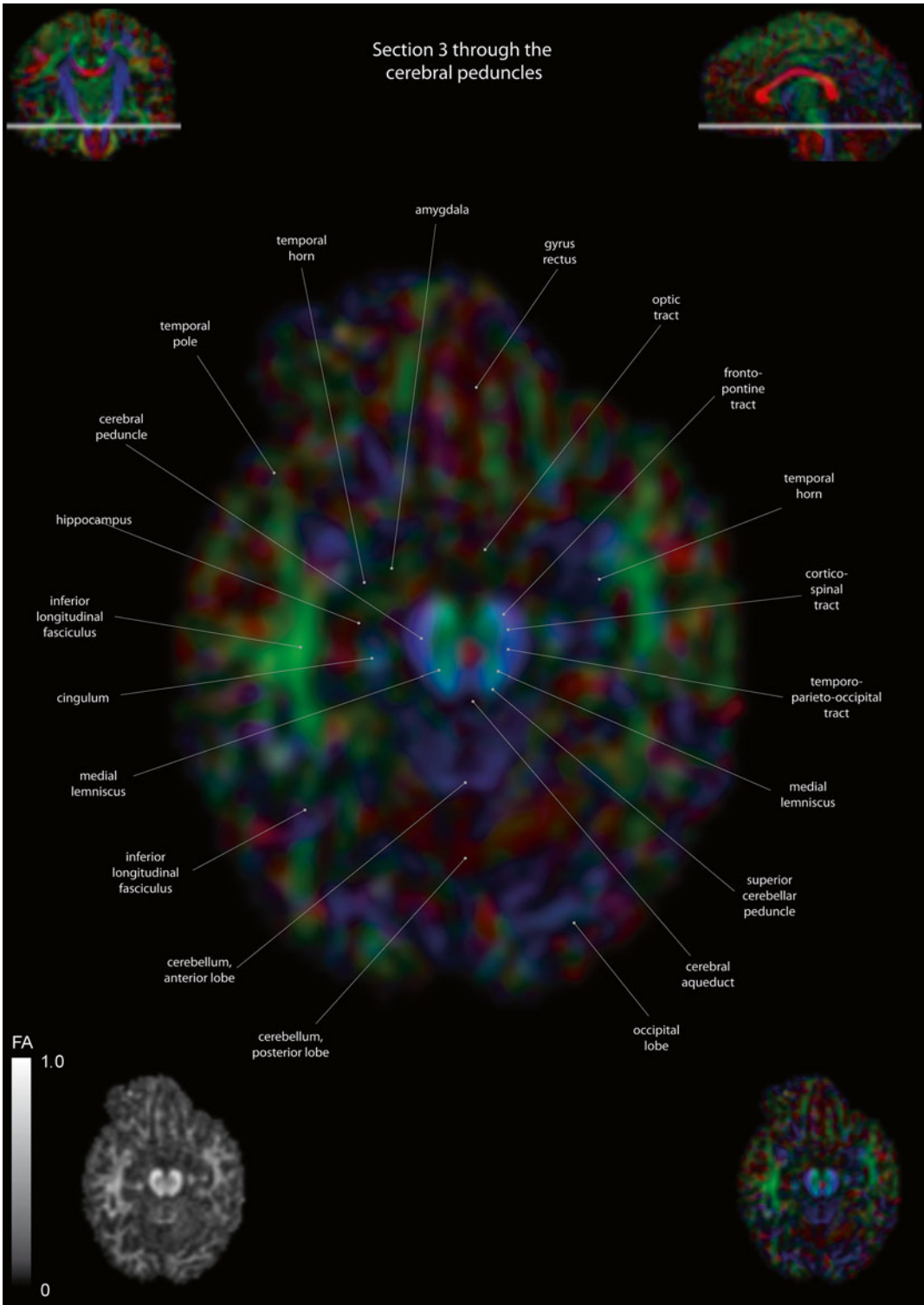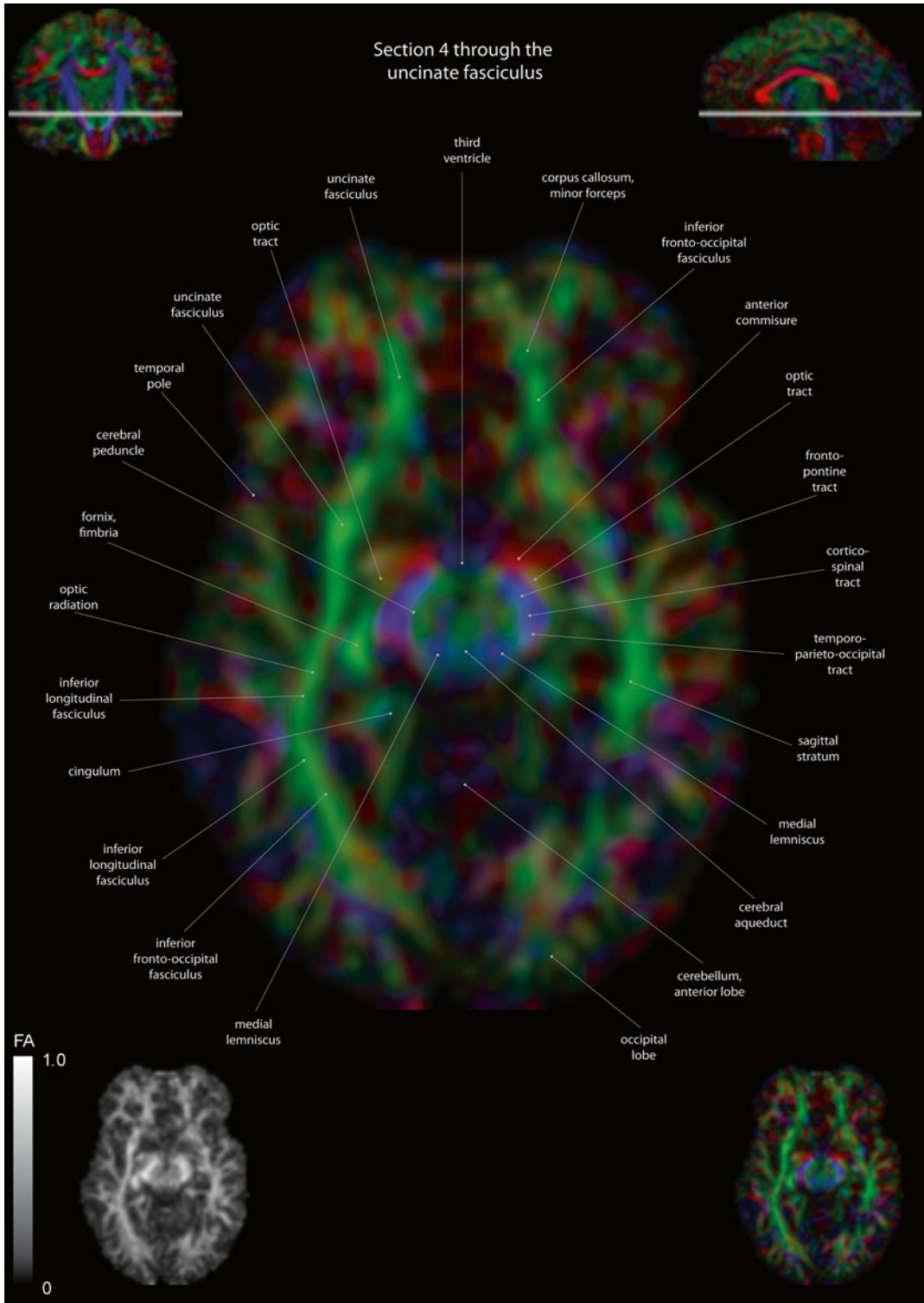
Fig. 12.3 Axial slices of a color-coded diffusion tensor image. The colors represent fiber direction; *red*=left to right, *blue*=cranio-caudal, and *green*=anterior-posterior. The intensity represents the fractional anisotropy (FA) also indicated in the *lower corner*. In the *upper corners*, the slice section is indicated in the coronal and sagittal plane
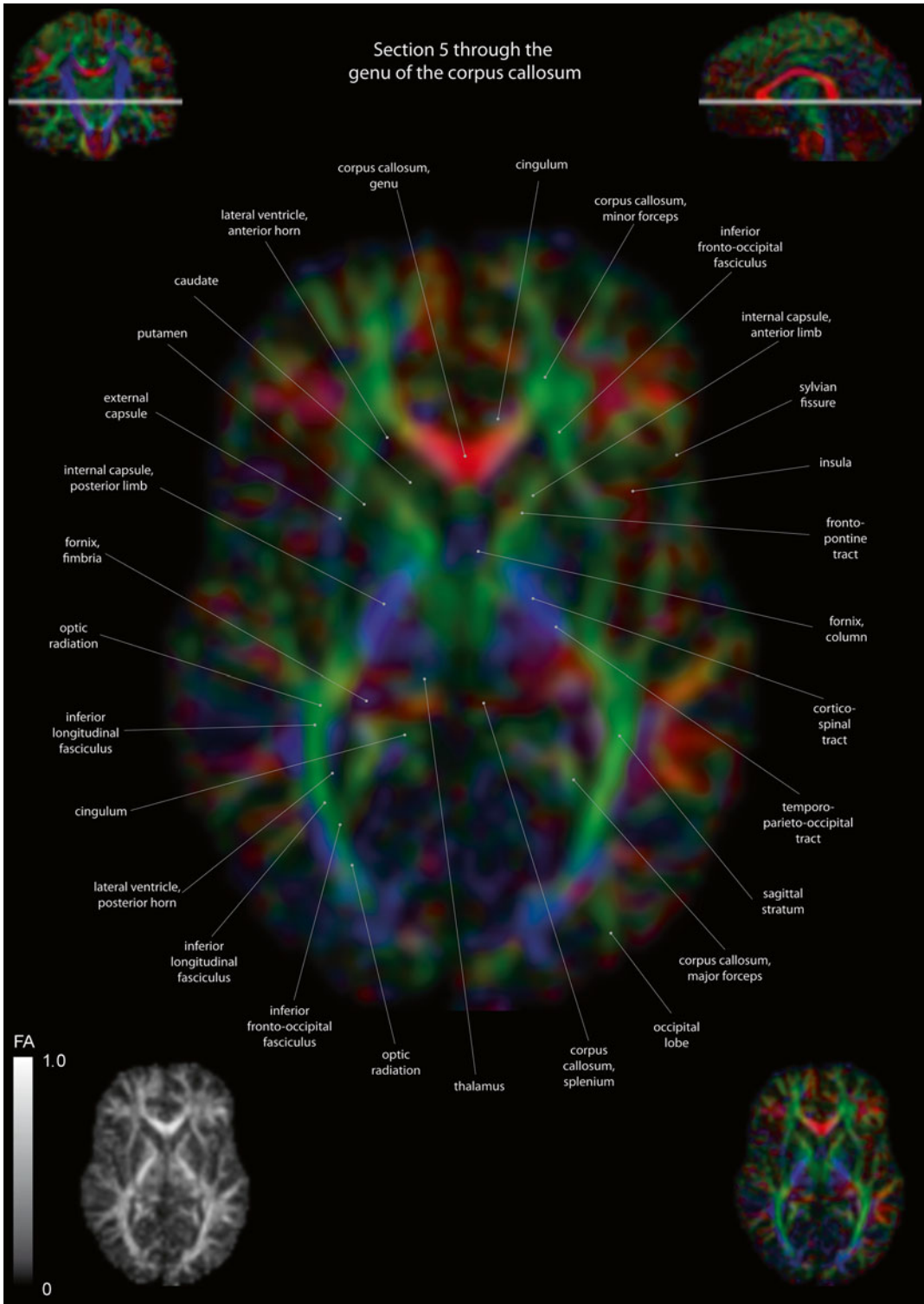
Fig. 12.4 Axial slices of a color-coded diffusion tensor image. The colors represent fiber direction; *red*=left to right, *blue*=cranio-caudal, and *green*=anterior-posterior. The intensity represents the fractional anisotropy (FA) also indicated in the *lower corner*. In the *upper corners*, the slice section is indicated in the coronal and sagittal plane
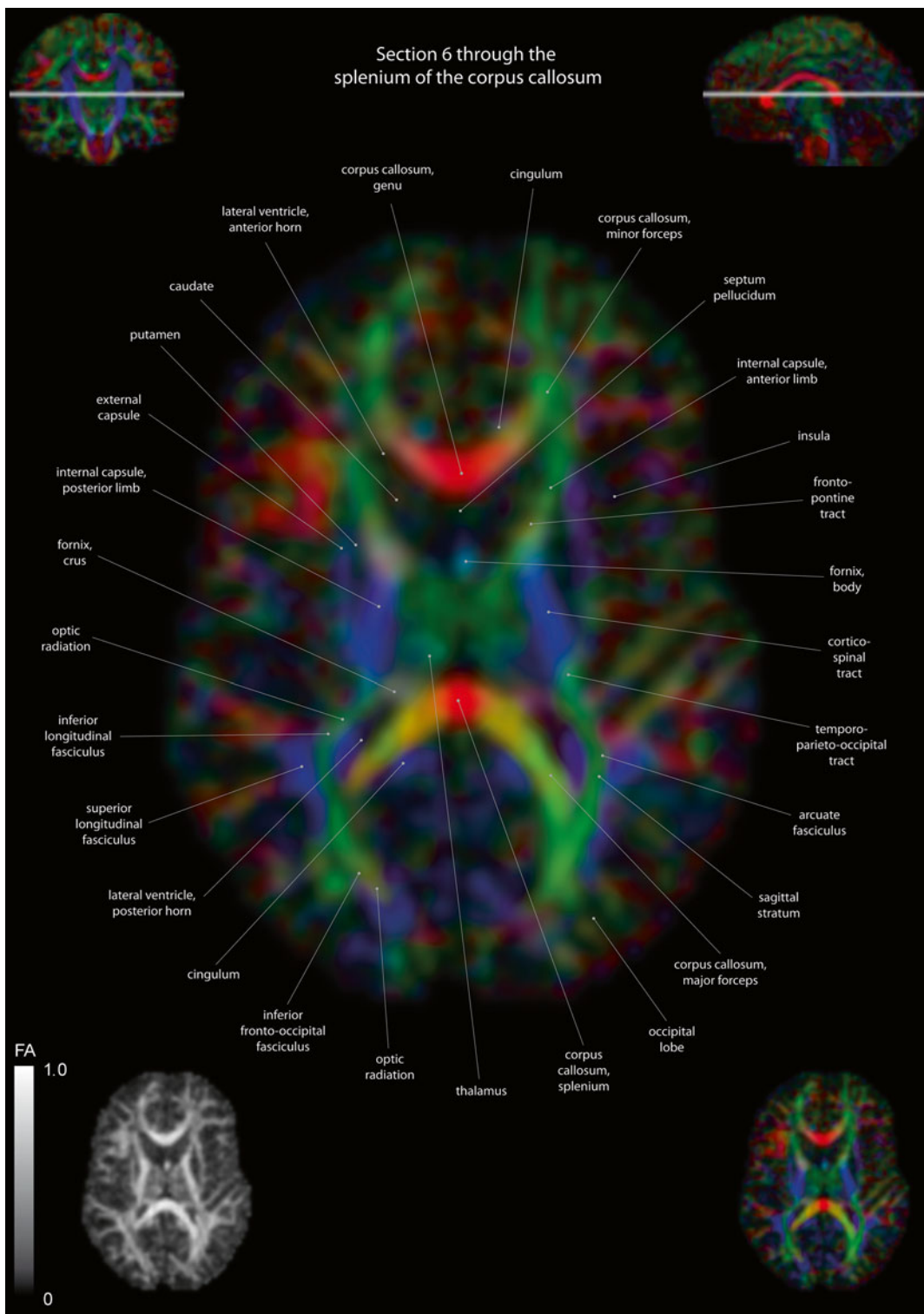
Fig. 12.5 Axial slices of a color-coded diffusion tensor image. The colors represent fiber direction; *red*=left to right, *blue*=cranio-caudal, and *green*=anterior-posterior. The intensity represents the fractional anisotropy (FA) also indicated in the *lower corner*. In the *upper corners*, the slice section is indicated in the coronal and sagittal plane
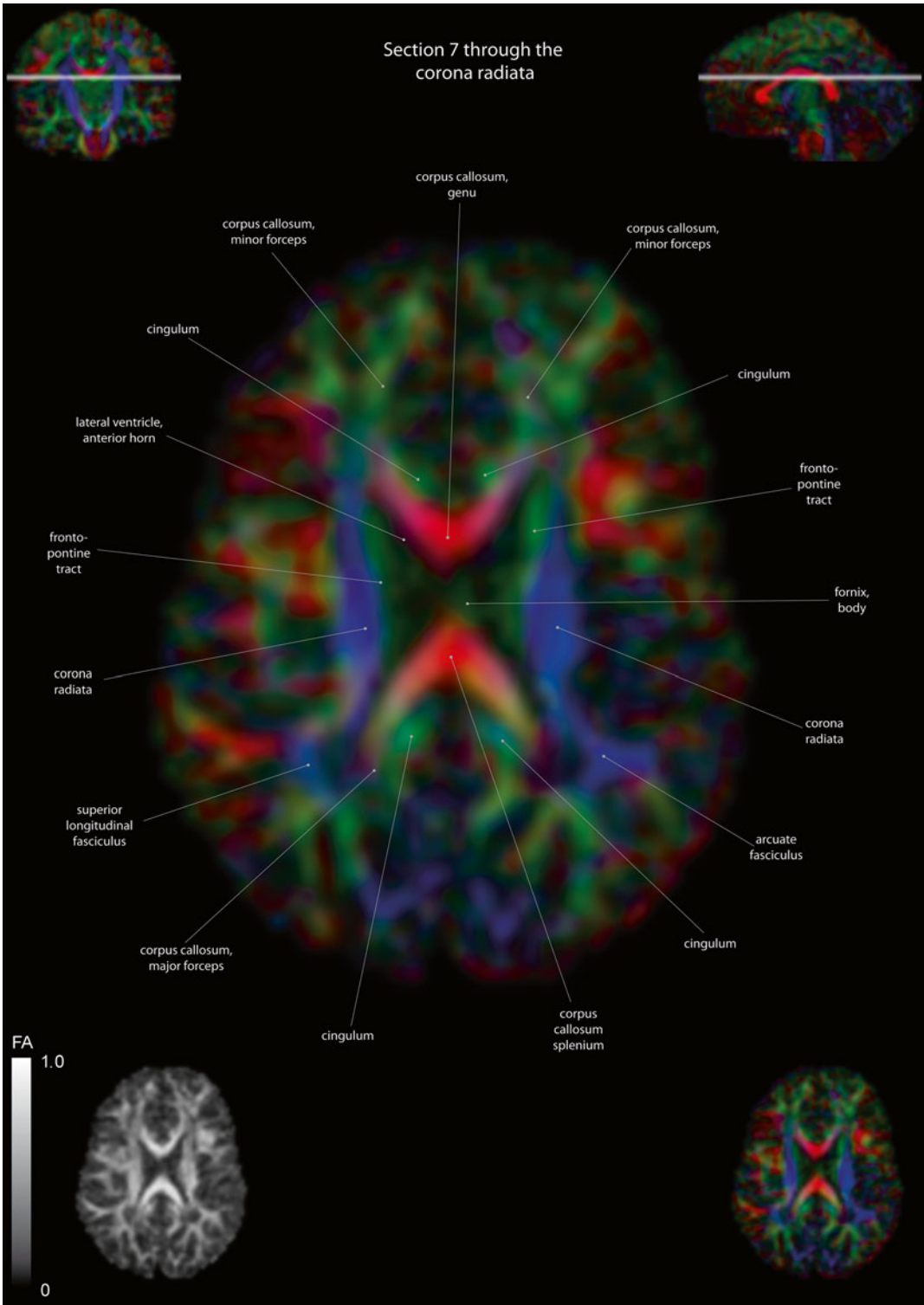
Fig. 12.6 Axial slices of a color-coded diffusion tensor image. The colors represent fiber direction; *red*=left to right, *blue*=cranio-caudal, and *green*=anterior-posterior. The intensity represents the fractional anisotropy (FA) also indicated in the *lower corner*. In the *upper corners*, the slice section is indicated in the coronal and sagittal plane
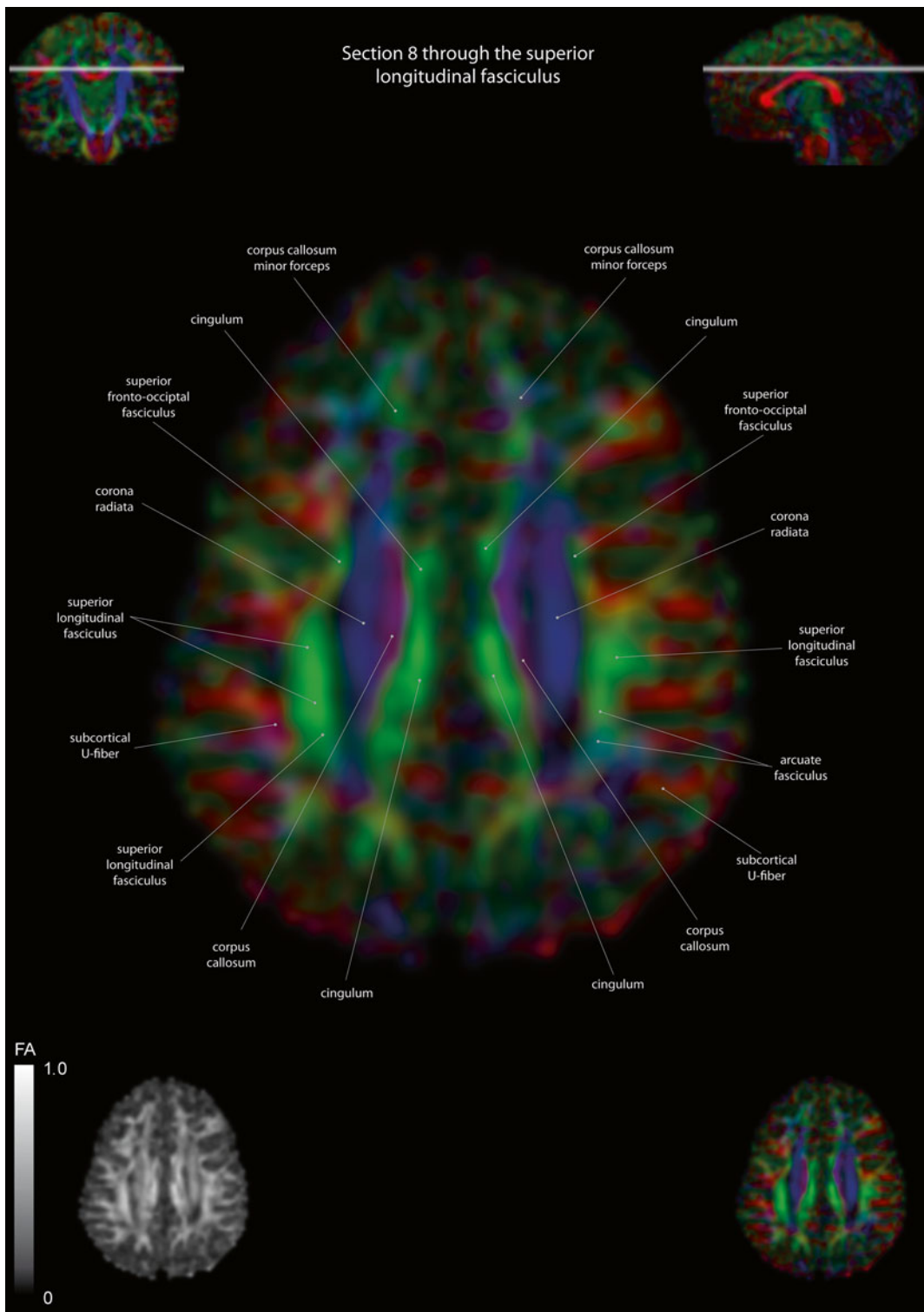
Fig. 12.7 Axial slices of a color-coded diffusion tensor image. The colors represent fiber direction; *red*=left to right, *blue*=cranio-caudal, and *green*=anterior-posterior. The intensity represents the fractional anisotropy (FA) also indicated in the *lower corner*. In the *upper corners*, the slice section is indicated in the coronal and sagittal plane

Fig. 12.8 Axial slices of a color-coded diffusion tensor image. The colors represent fiber direction; *red* = left to right, *blue* = cranio-caudal, and *green* = anterior-posterior. The intensity represents the fractional anisotropy (FA) also indicated in the *lower corner*. In the *upper corners*, the slice section is indicated in the coronal and sagittal plane
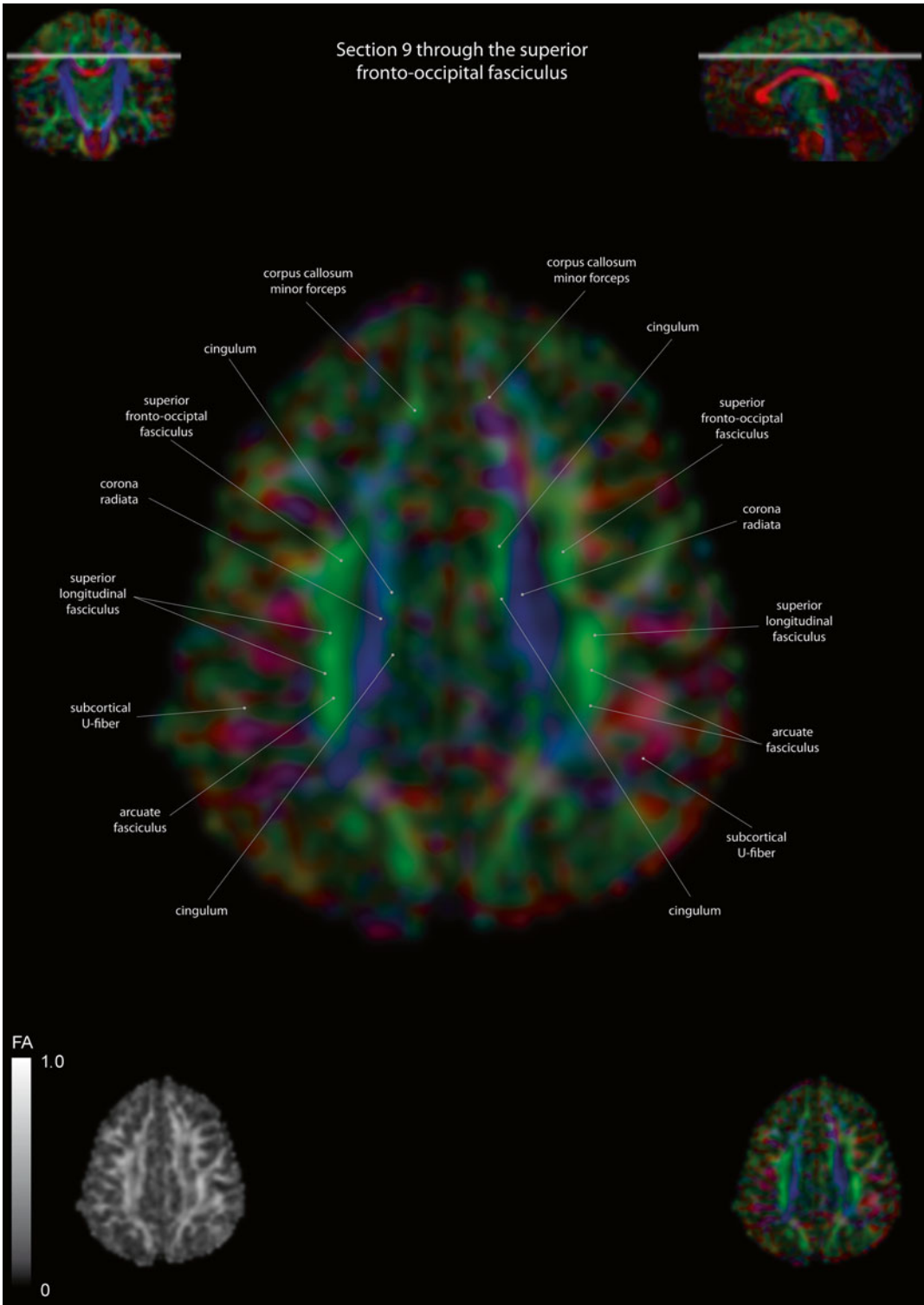
Fig. 12.9 Axial slices of a color-coded diffusion tensor image. The colors represent fiber direction; *red* = left to right, *blue* = cranio-caudal, and *green* = anterior-posterior. The intensity represents the fractional anisotropy (FA) also indicated in the *lower corner*. In the *upper corners*, the slice section is indicated in the coronal and sagittal plane
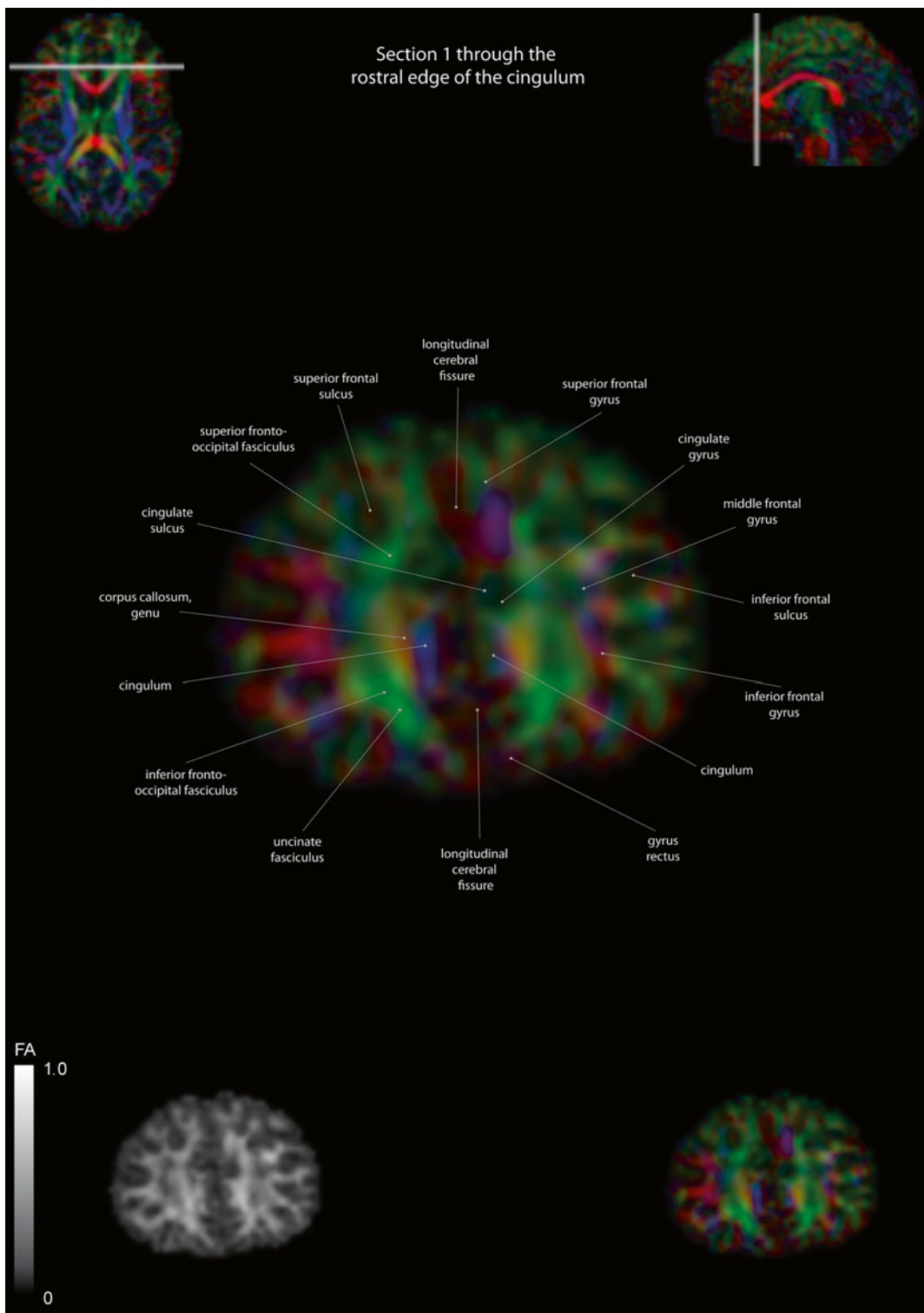
Fig. 12.10 Axial slices of a color-coded diffusion tensor image. The colors represent fiber direction; *red*=left to right, *blue*=cranio-caudal, and *green*=anterior-posterior. The intensity represents the fractional anisotropy (FA) also indicated in the *lower corner*. In the *upper corners*, the slice section is indicated in the coronal and sagittal plane
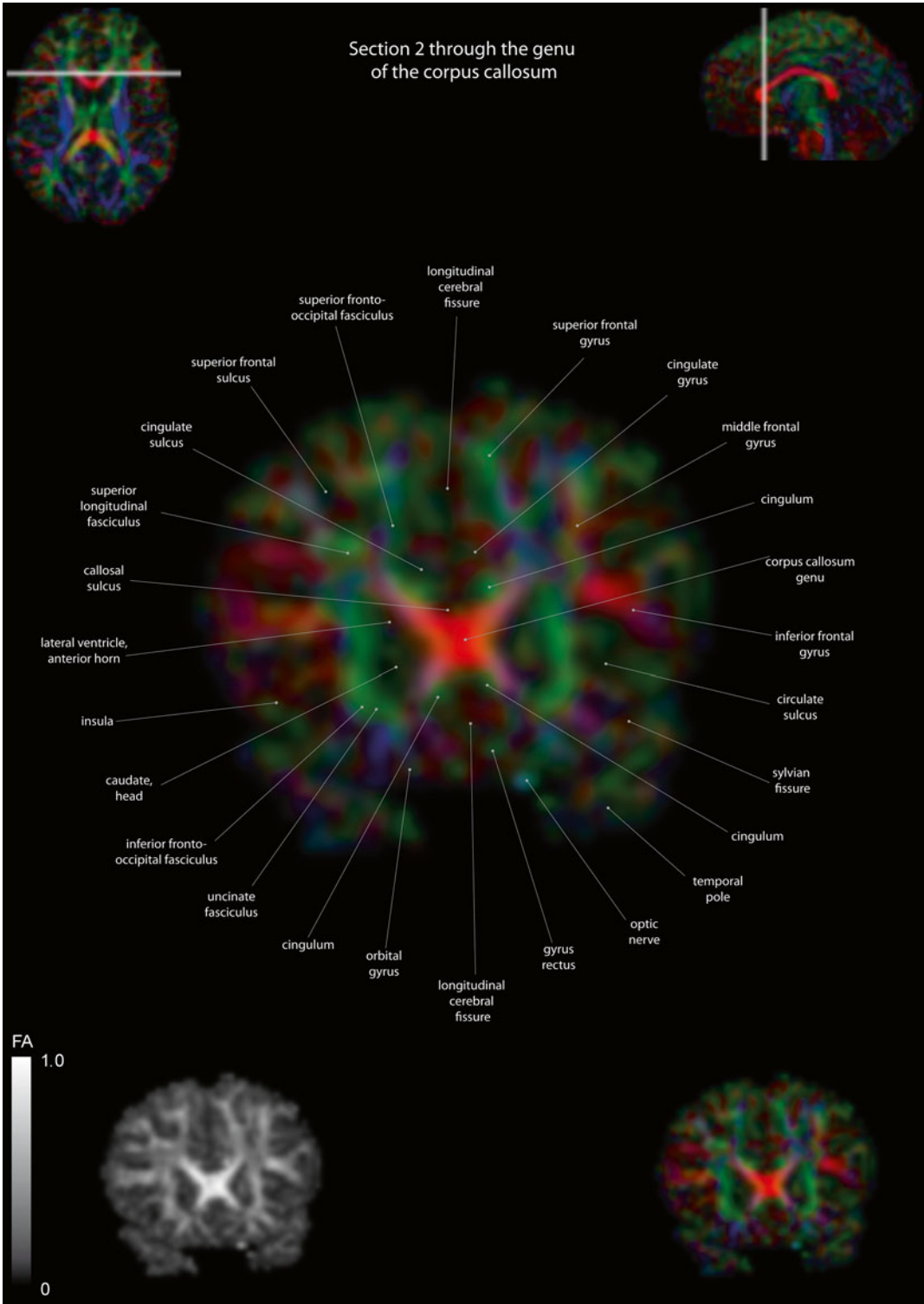
Fig. 12.11 Coronal slices of a color-coded diffusion tensor image. The colors represent fiber direction; *red* = left to right, *blue* = cranio-caudal, and *green* = anterior-posterior. The intensity represents the fractional anisotropy (FA) also indicated in the *lower corner*. In the *upper corners*, the slice section is indicated in the axial and sagittal plane
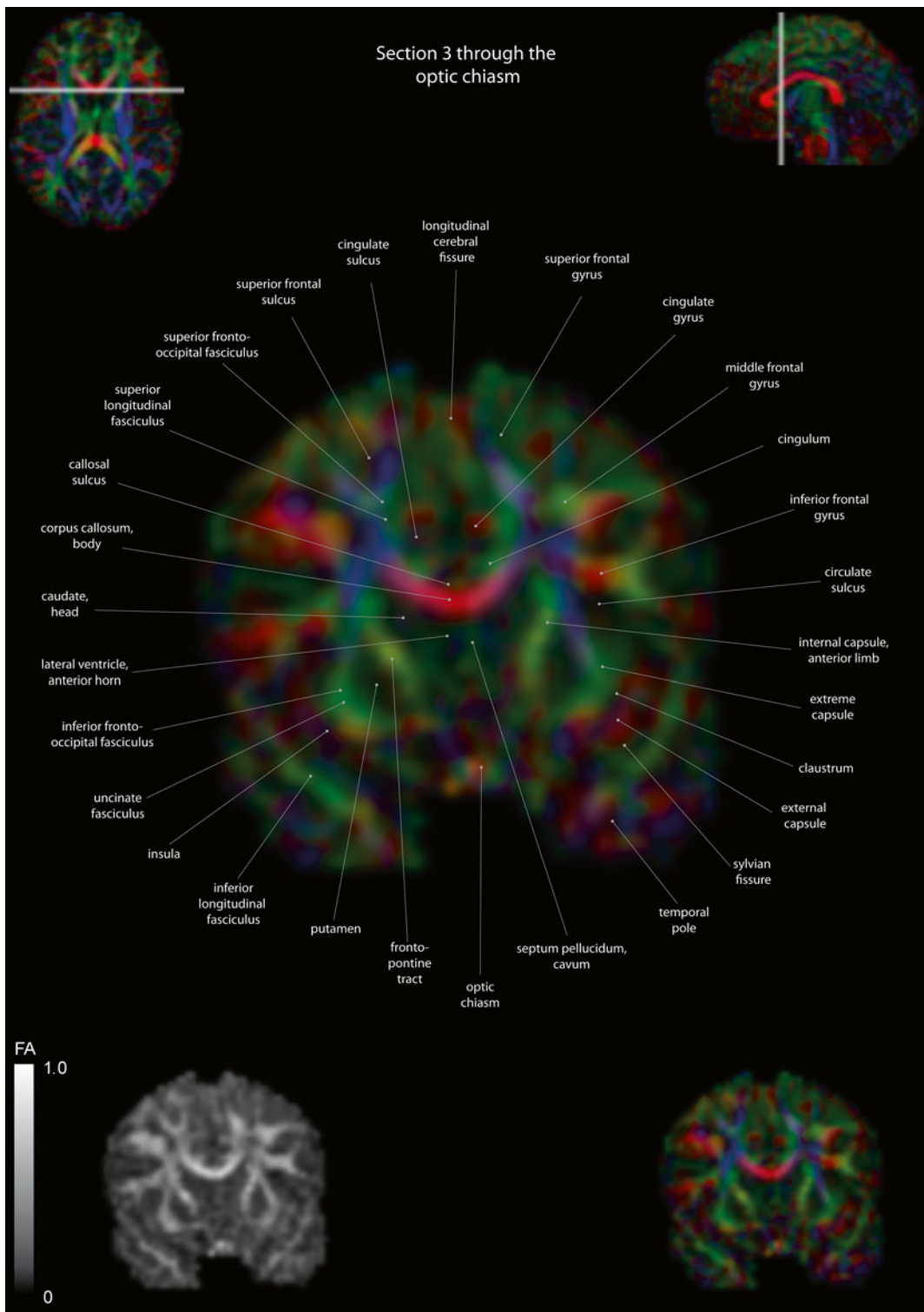
Fig. 12.12 Coronal slices of a color-coded diffusion tensor image. The colors represent fiber direction; *red* = left to right, *blue* = cranio-caudal, and *green* = anterior-posterior. The intensity represents the fractional anisotropy (FA) also indicated in the *lower corner*. In the *upper corners*, the slice section is indicated in the axial and sagittal plane
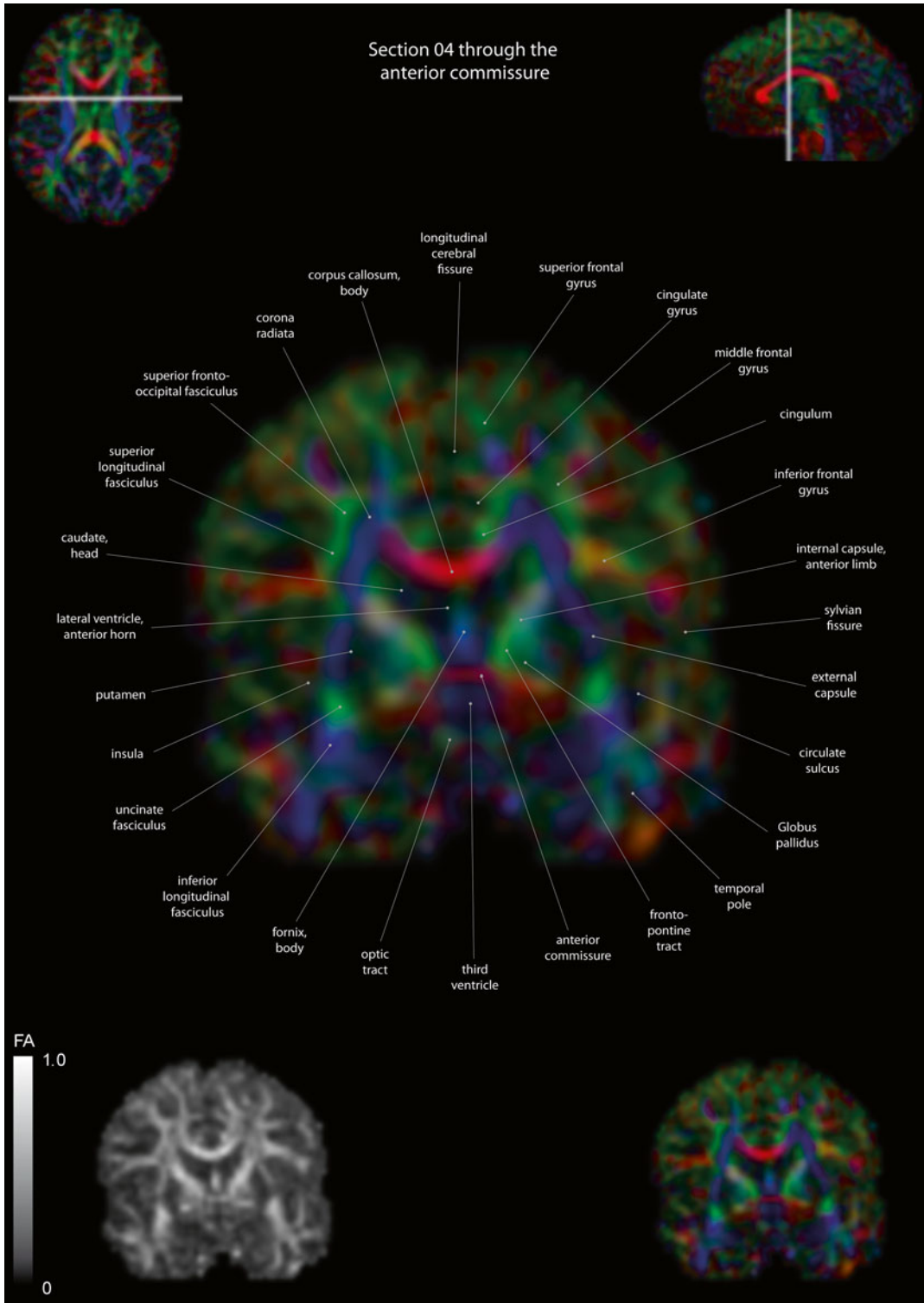
Fig. 12.13 Coronal slices of a color-coded diffusion tensor image. The colors represent fiber direction; *red*=left to right, *blue*=cranio-caudal, and *green*=anterior-posterior. The intensity represents the fractional anisotropy (FA) also indicated in the *lower corner*. In the *upper corners*, the slice section is indicated in the axial and sagittal plane

Fig. 12.14 Coronal slices of a color-coded diffusion tensor image. The colors represent fiber direction; *red*=left to right, *blue*=cranio-caudal, and *green*=anterior-posterior. The intensity represents the fractional anisotropy (FA) also indicated in the *lower corner*. In the *upper corners*, the slice section is indicated in the axial and sagittal plane
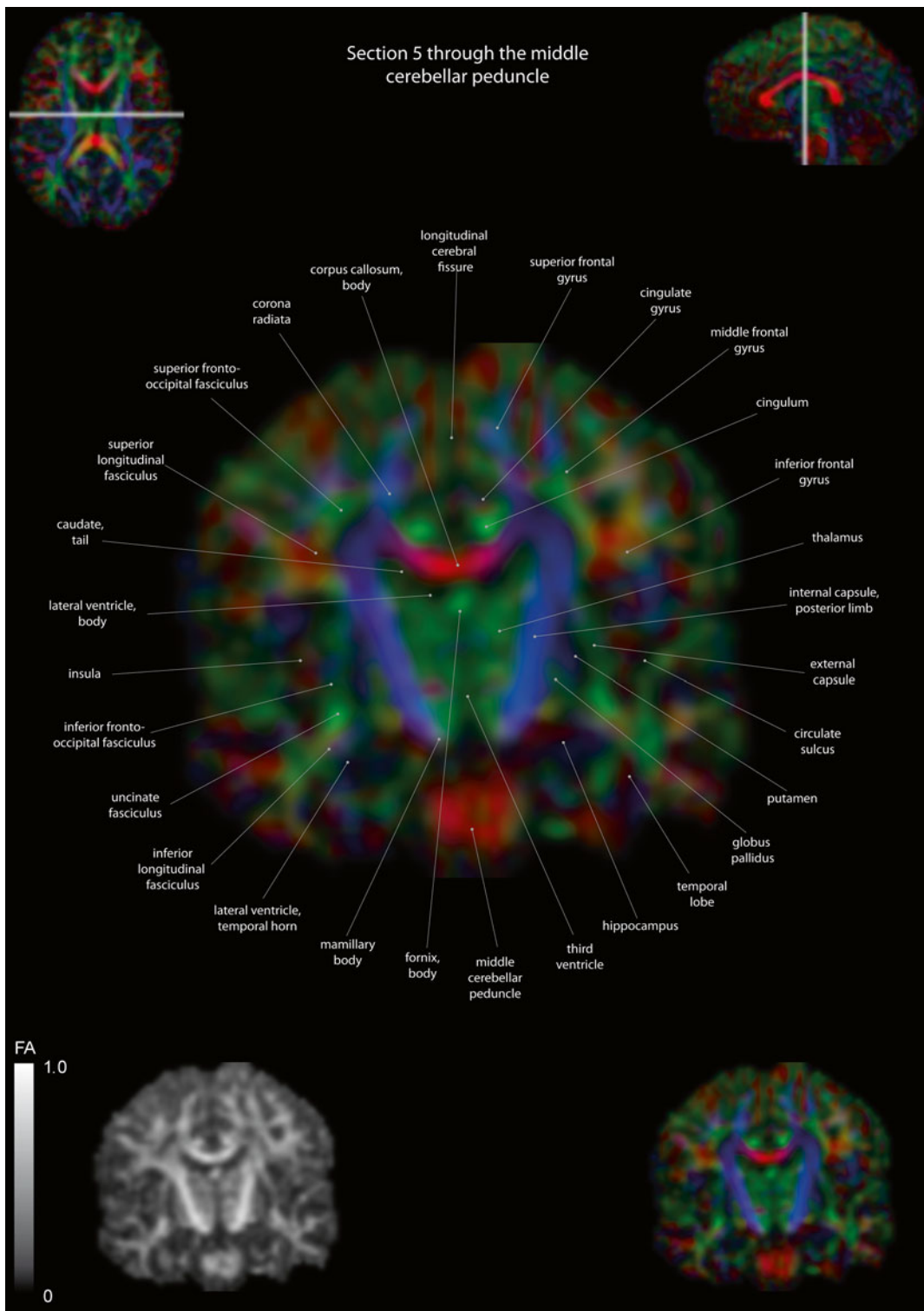
Fig. 12.15 Coronal slices of a color-coded diffusion tensor image. The colors represent fiber direction; *red*=left to right, *blue*=cranio-caudal, and *green*=anterior-posterior. The intensity represents the fractional anisotropy (FA) also indicated in the *lower corner*. In the *upper corners*, the slice section is indicated in the axial and sagittal plane
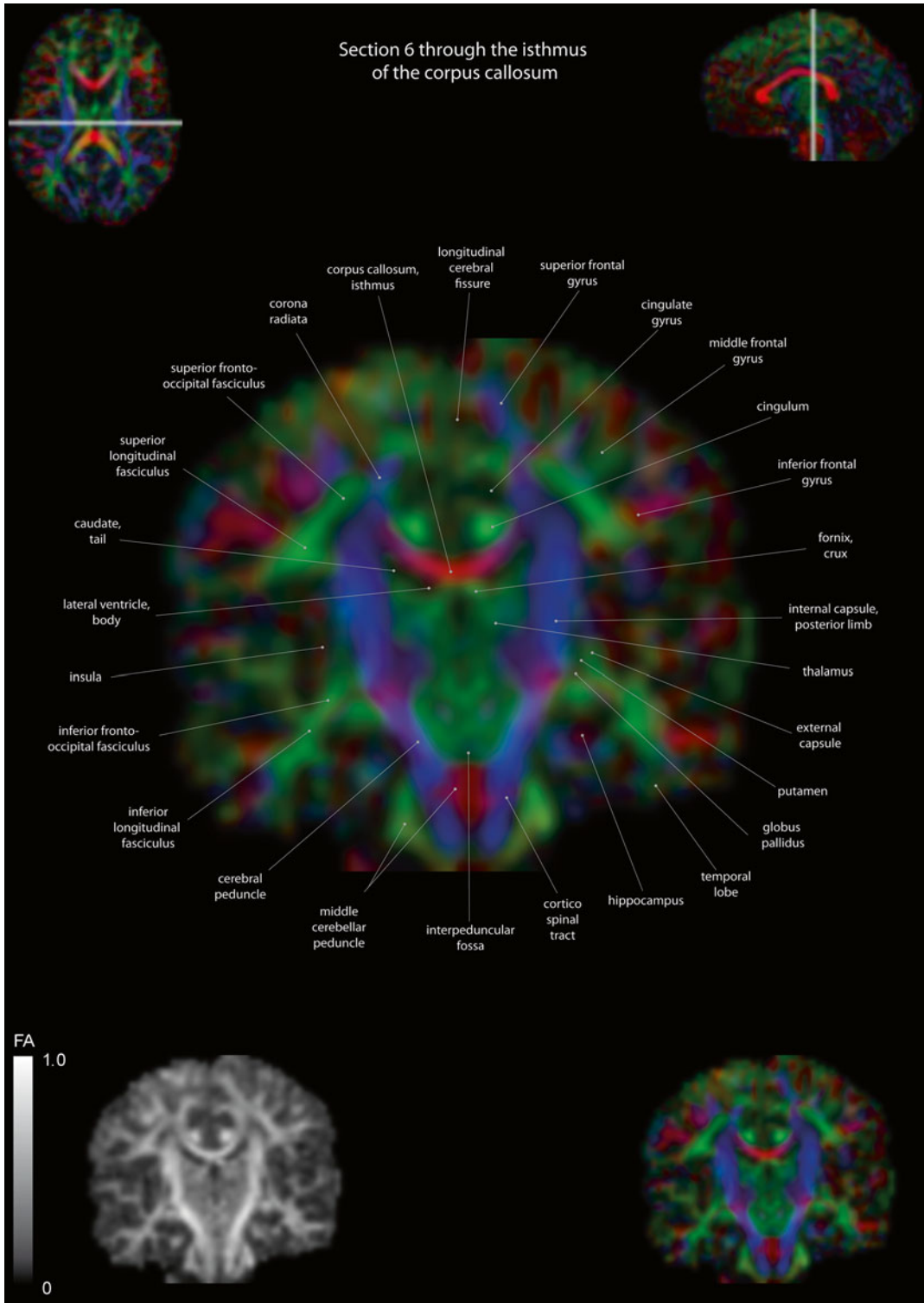
Fig. 12.16 Coronal slices of a color-coded diffusion tensor image. The colors represent fiber direction; *red* = left to right, *blue* = cranio-caudal, and *green* = anterior-posterior. The intensity represents the fractional anisotropy (FA) also indicated in the *lower corner*. In the *upper corners*, the slice section is indicated in the axial and sagittal plane
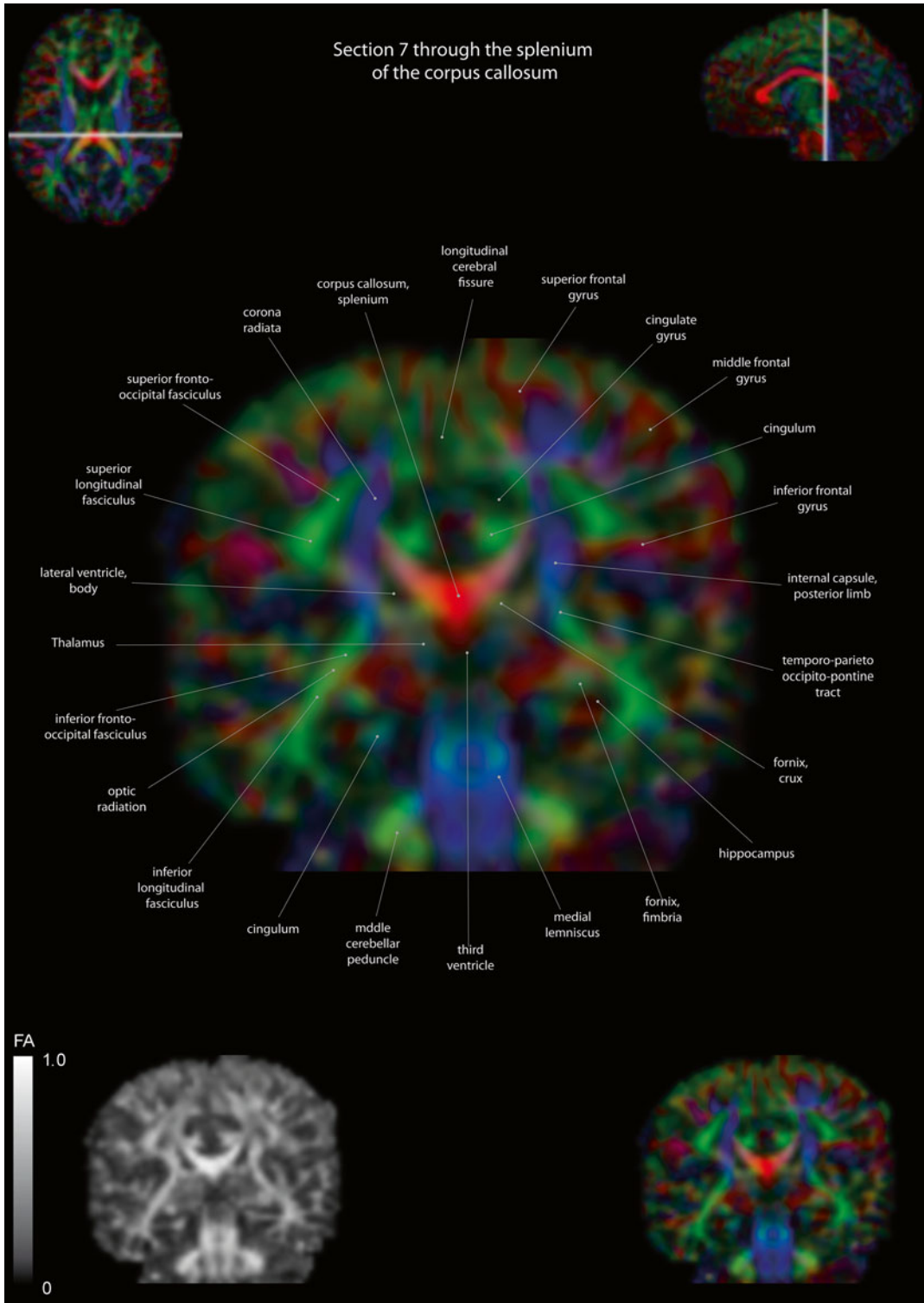
Fig. 12.17 Coronal slices of a color-coded diffusion tensor image. The colors represent fiber direction; *red* = left to right, *blue* = cranio-caudal, and *green* = anterior-posterior. The intensity represents the fractional anisotropy (FA) also indicated in the *lower corner*. In the *upper corners*, the slice section is indicated in the axial and sagittal plane
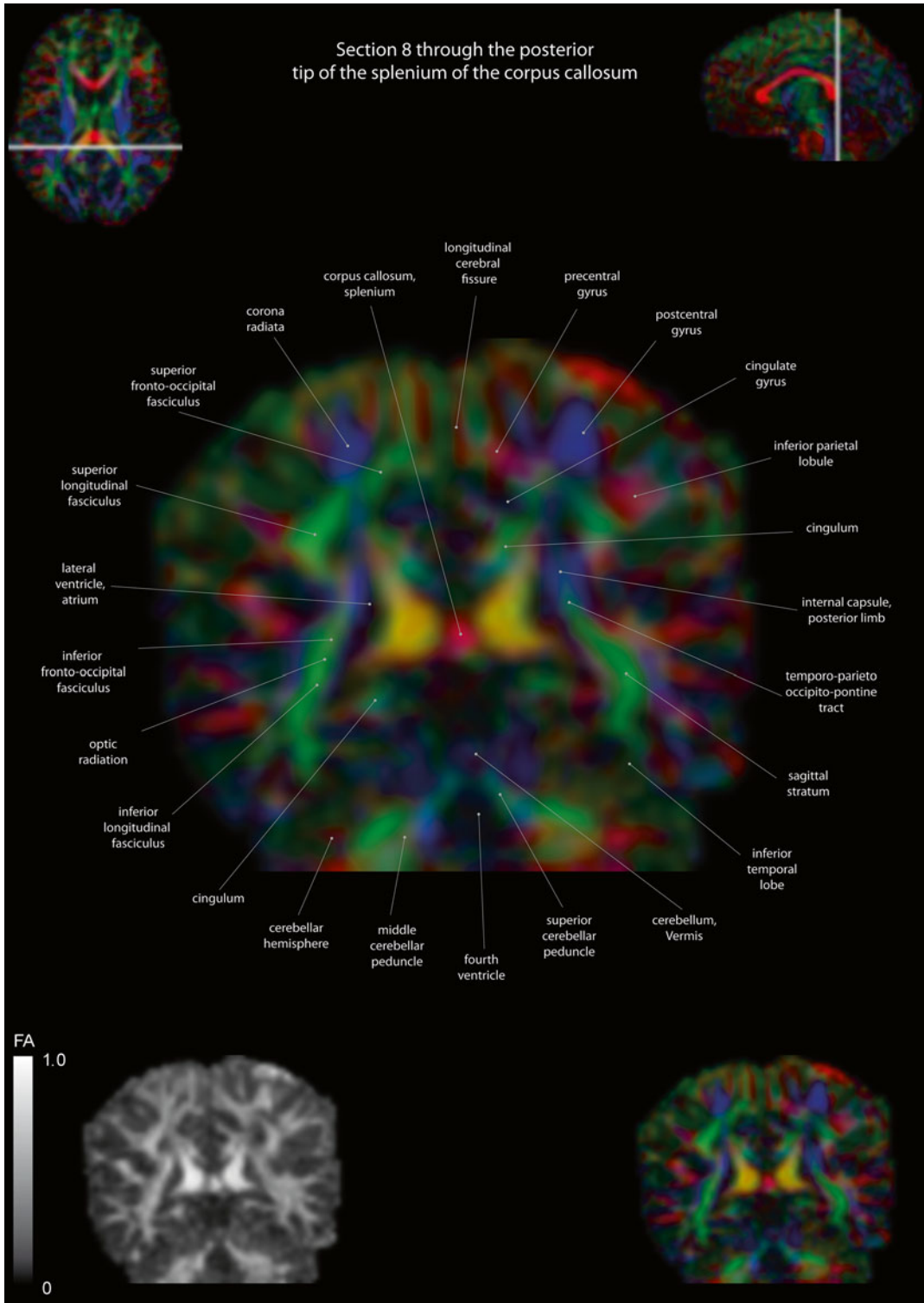
Fig. 12.18 Coronal slices of a color-coded diffusion tensor image. The colors represent fiber direction; *red* = left to right, *blue* = cranio-caudal, and *green* = anterior-posterior. The intensity represents the fractional anisotropy (FA) also indicated in the *lower corner*. In the *upper corners*, the slice section is indicated in the axial and sagittal plane
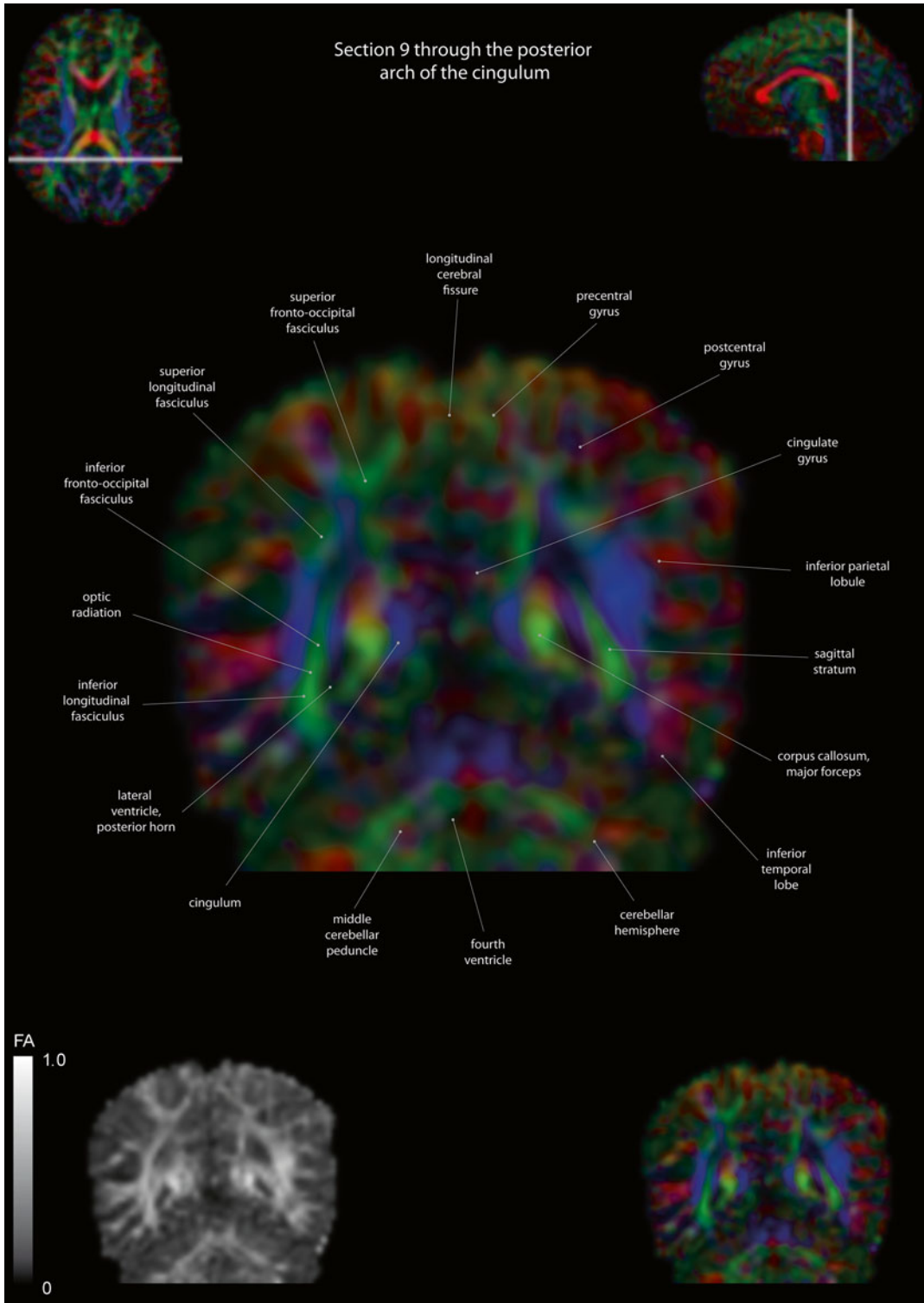
Fig. 12.19 Coronal slices of a color-coded diffusion tensor image. The colors represent fiber direction; *red* = left to right, *blue* = cranio-caudal, and *green* = anterior-posterior. The intensity represents the fractional anisotropy (FA) also indicated in the *lower corner*. In the *upper corners*, the slice section is indicated in the axial and sagittal plane
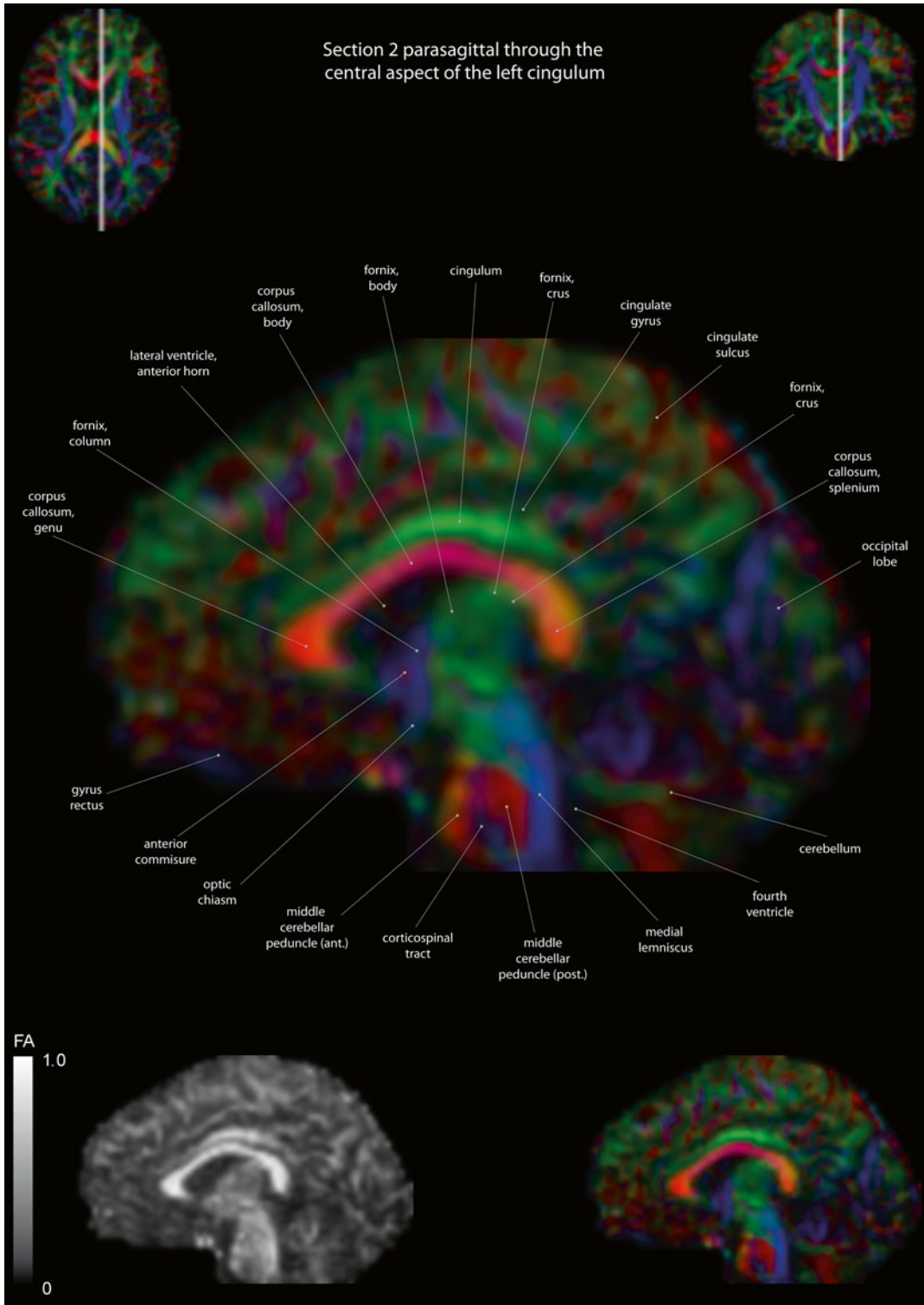
Fig. 12.20 Sagittal slices of a color-coded diffusion tensor image. The colors represent fiber direction; *red*=left to right, *blue*=cranio-caudal, and *green*=anterior-posterior. The intensity represents the fractional anisotropy (FA) also indicated in the *lower corner*. In the *upper corners*, the slice section is indicated in the axial and coronal plane

Fig. 12.21 Sagittal slices of a color-coded diffusion tensor image. The colors represent fiber direction; *red*=left to right, *blue*=cranio-caudal, and *green*=anterior-posterior. The intensity represents the fractional anisotropy (FA) also indicated in the *lower corner*. In the *upper corners*, the slice section is indicated in the axial and coronal plane
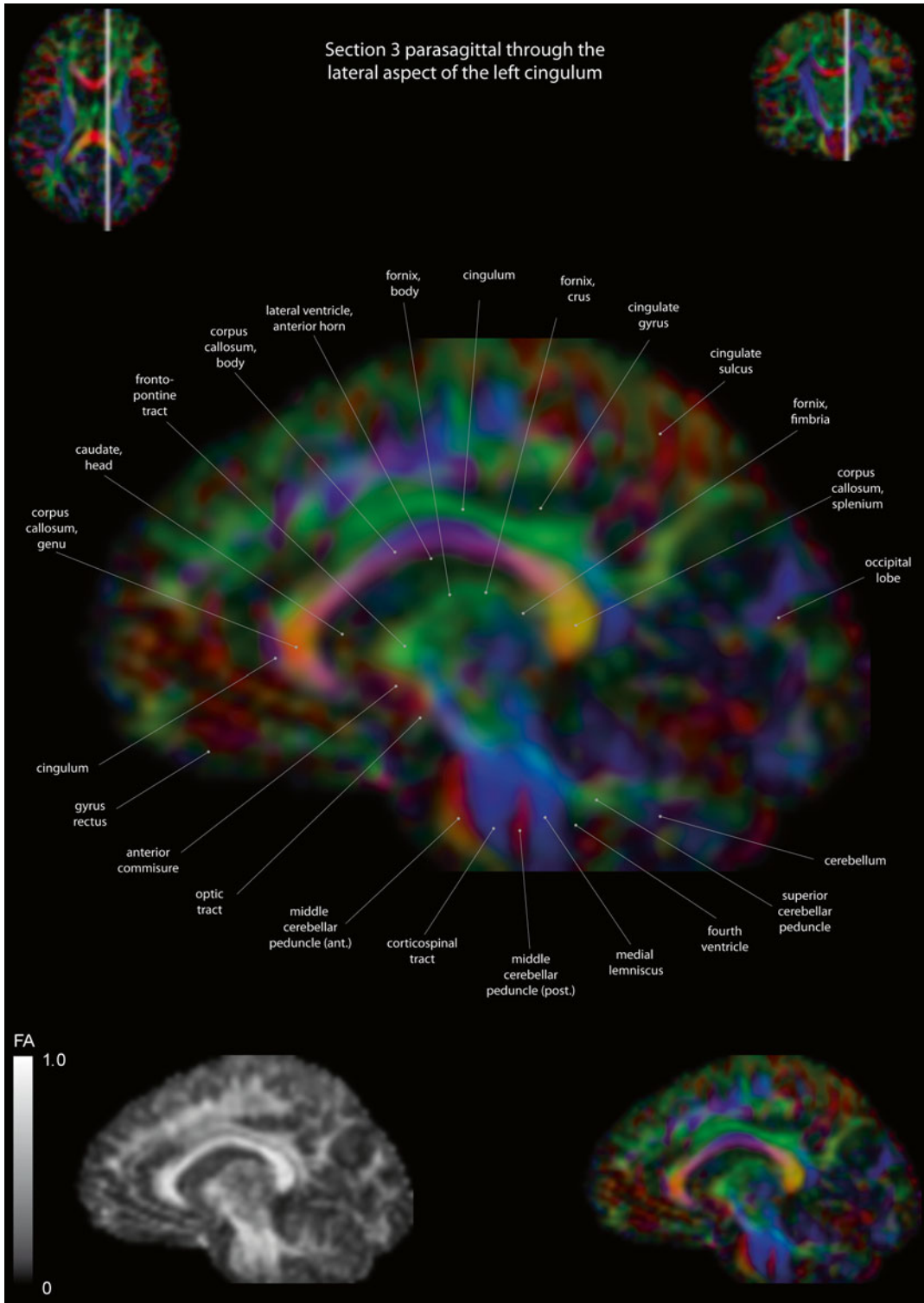
Fig. 12.22 Sagittal slices of a color-coded diffusion tensor image. The colors represent fiber direction; *red* = left to right, *blue* = cranio-caudal, and *green* = anterior-posterior. The intensity represents the fractional anisotropy (FA) also indicated in the *lower corner*. In the *upper corners*, the slice section is indicated in the axial and coronal plane
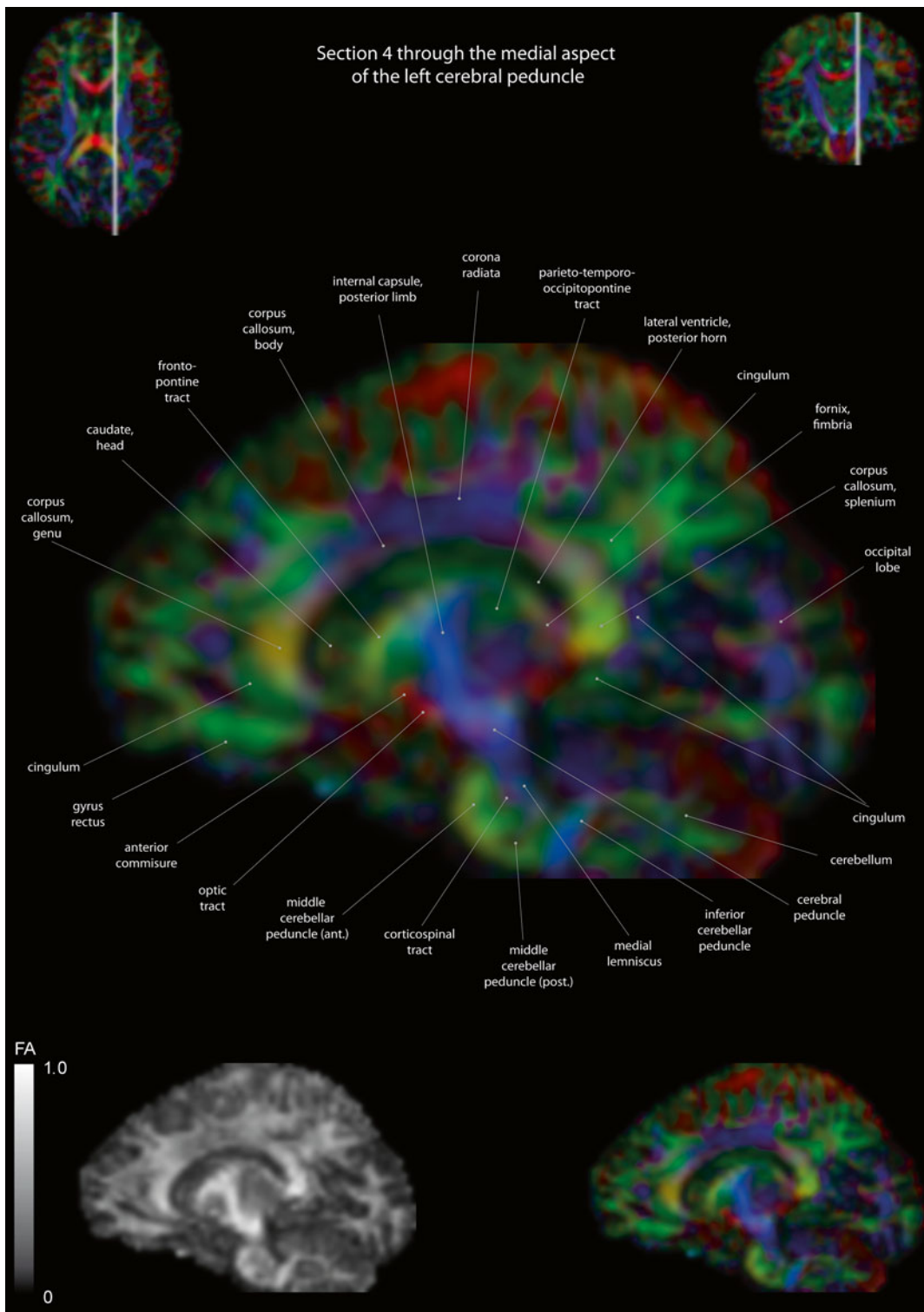
Fig. 12.23 Sagittal slices of a color-coded diffusion tensor image. The colors represent fiber direction; *red*=left to right, *blue*=cranio-caudal, and *green*=anterior-posterior. The intensity represents the fractional anisotropy (FA) also indicated in the *lower corner*. In the *upper corners*, the slice section is indicated in the axial and coronal plane
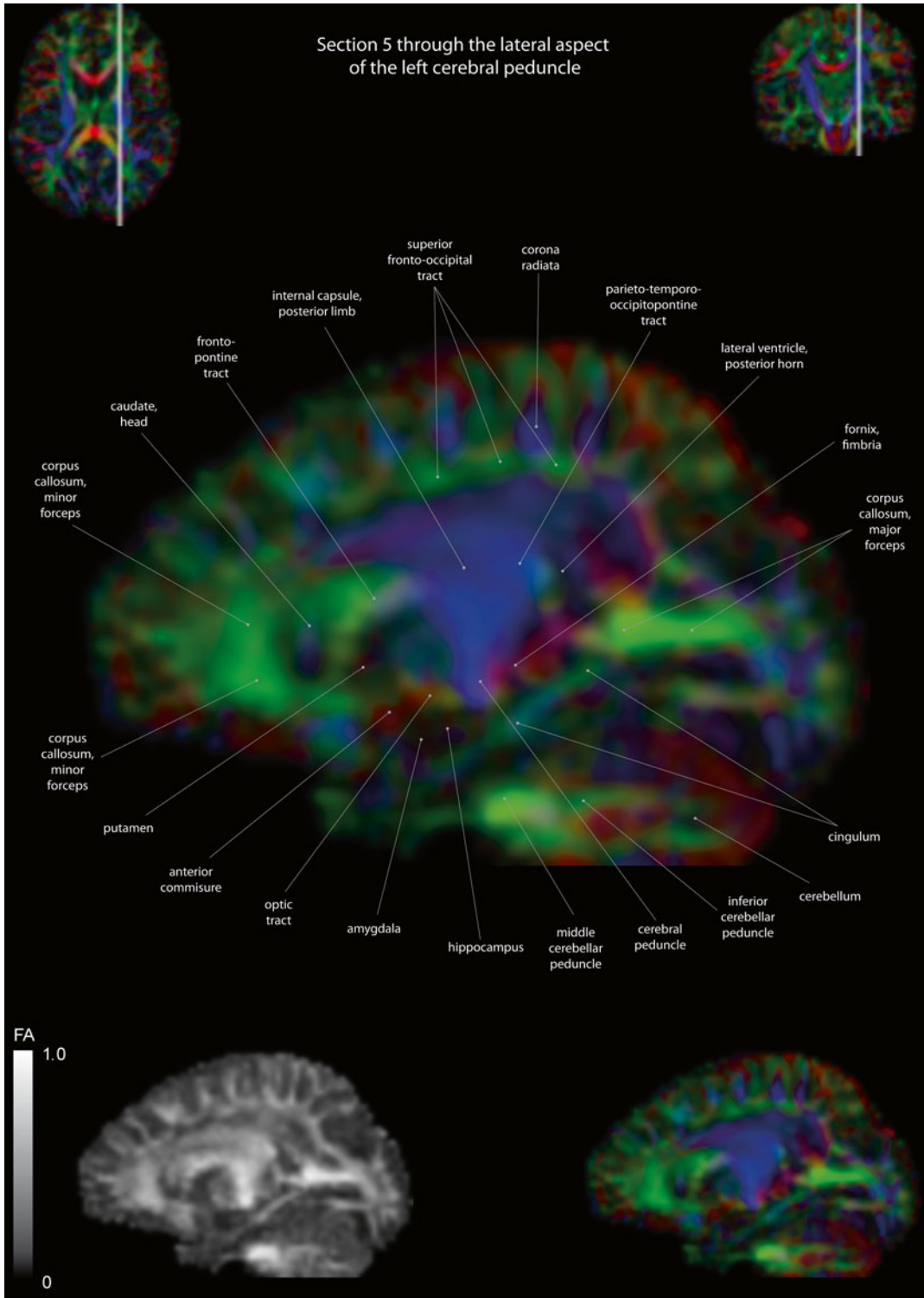
Fig. 12.24 Sagittal slices of a color-coded diffusion tensor image. The colors represent fiber direction; *red* = left to right, *blue* = cranio-caudal, and *green* = anterior-posterior. The intensity represents the fractional anisotropy (FA) also indicated in the *lower corner*. In the *upper corners*, the slice section is indicated in the axial and coronal plane
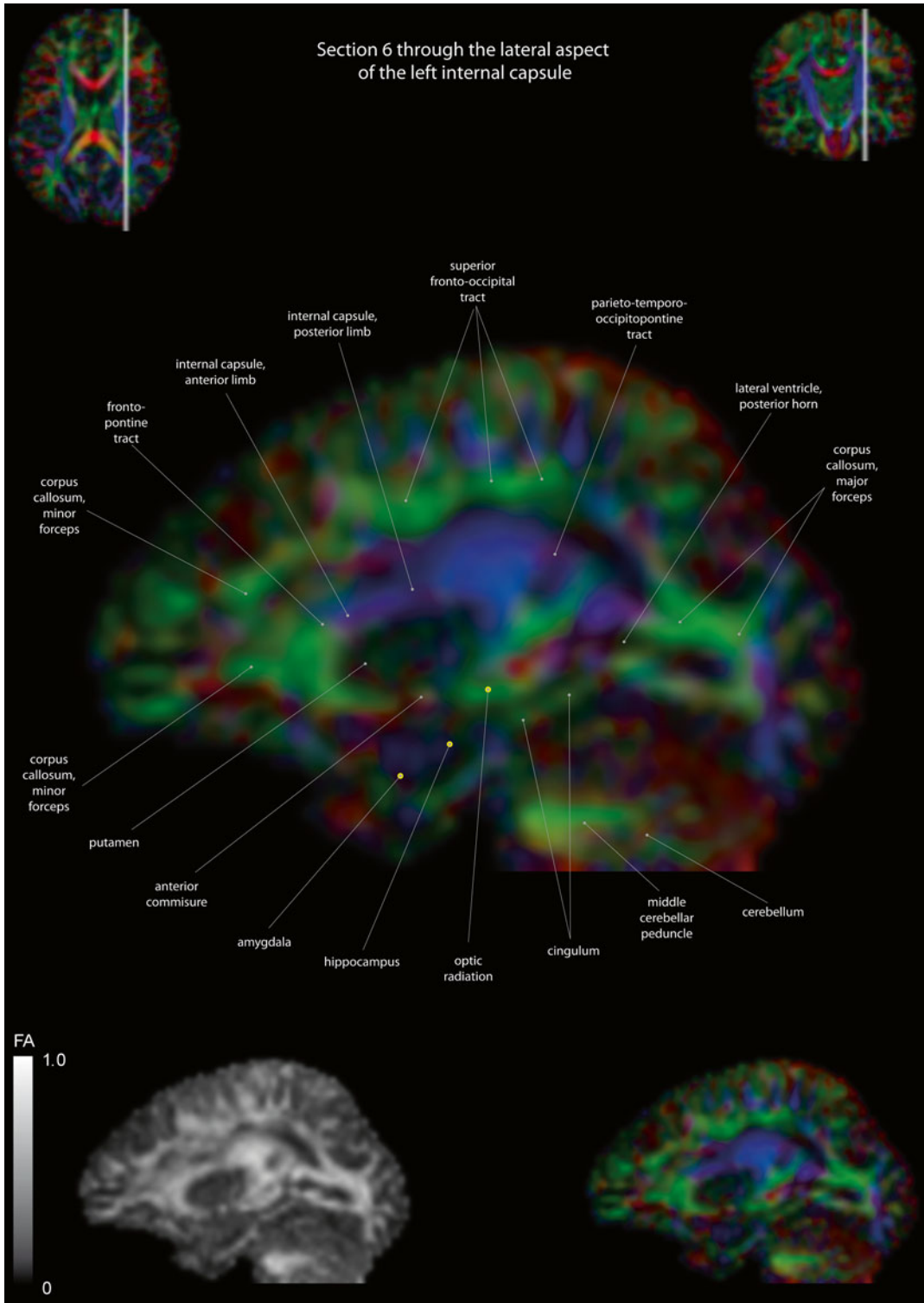
Fig. 12.25 Sagittal slices of a color-coded diffusion tensor image. The colors represent fiber direction; *red*=left to right, *blue*=cranio-caudal, and *green*=anterior-posterior. The intensity represents the fractional anisotropy (FA) also indicated in the *lower corner*. In the *upper corners*, the slice section is indicated in the axial and coronal plane

Fig. 12.26 Sagittal slices of a color-coded diffusion tensor image. The colors represent fiber direction; *red* = left to right, *blue* = cranio-caudal, and *green* = anterior-posterior. The intensity represents the fractional anisotropy (FA) also indicated in the *lower corner*. In the *upper corners*, the slice section is indicated in the axial and coronal plane
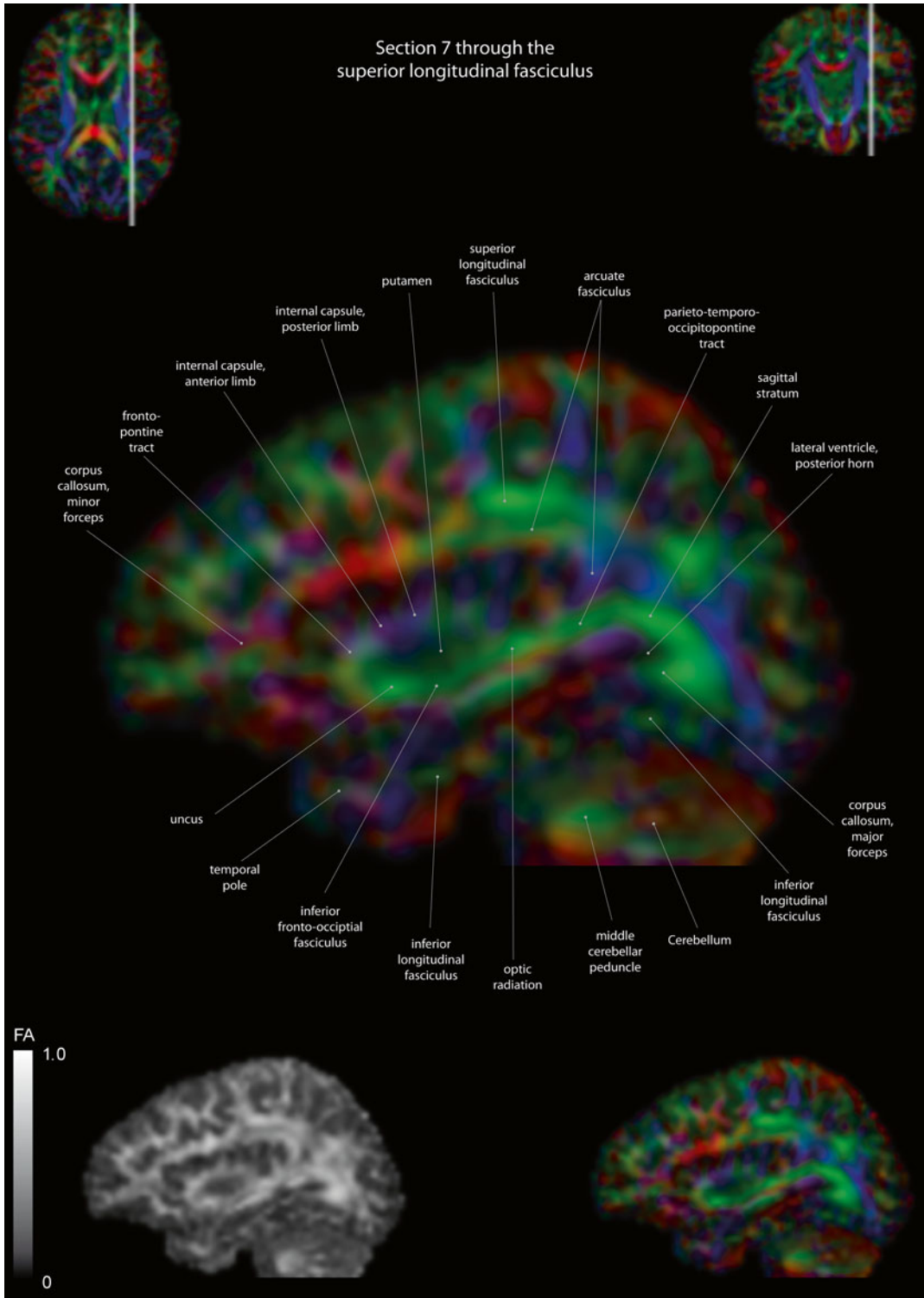
Fig. 12.27 Sagittal slices of a color-coded diffusion tensor image. The colors represent fiber direction; *red* = left to right, *blue* = cranio-caudal, and *green* = anterior-posterior. The intensity represents the fractional anisotropy (FA) also indicated in the *lower corner*. In the *upper corners*, the slice section is indicated in the axial and coronal plane
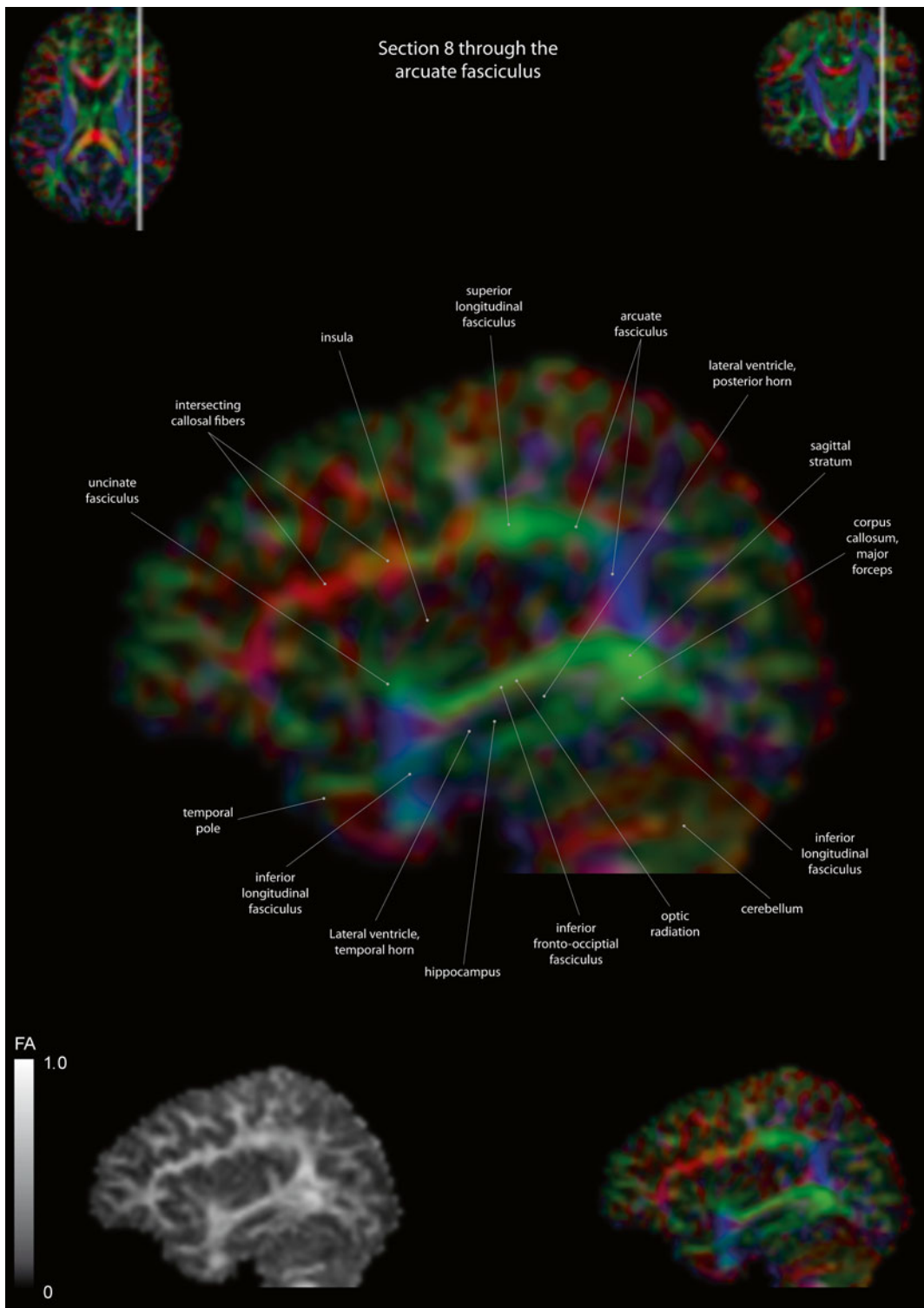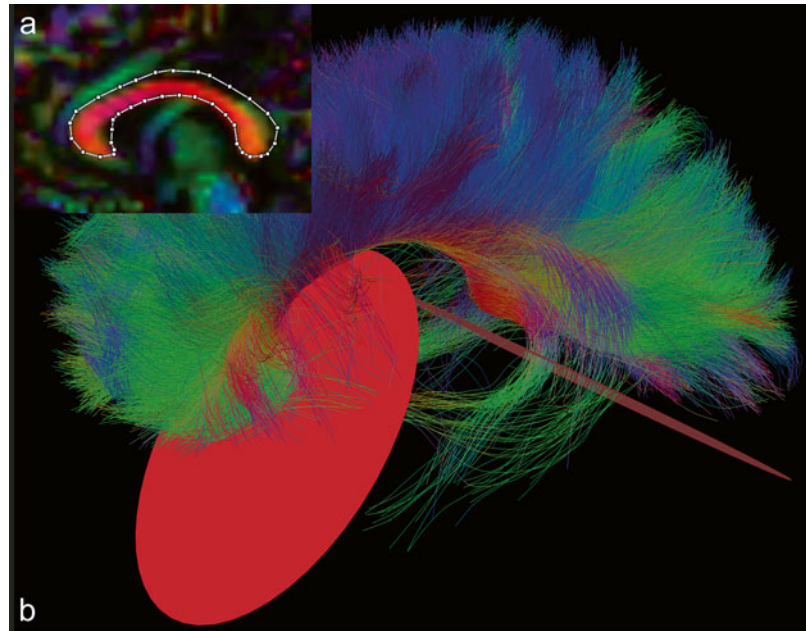
Fig. 12.28 Tracking of the Corpus callosum (CC), first step. (**a**) Midsagittal view of the CC with the initial starting region of interest (ROI) in *white*. (**b**) Removal of spurious fibers mainly from the cingulum using exclusion ROIs (*red*)

tal plane (Fig. 12.28a). The corpus callosum appears as a central large red structure. Outline the structure (white outline) and you should yield an initial tracking result that appears similar to Fig. 12.28b. Since the cingulum and the fornix run directly adjacent to the corpus callosum in the midsagittal plane, parts of these tracts are included in the initial result. These spurious tracts can be removed by placement of two ROIs (red ROIs, Fig. 12.28b). The first ROI is placed just posteriorly of the caudal tip of the genu of the corpus callosum (left red ROI) and the cingulum fibers from this ROI are excluded. The second ROI is placed anteriorly of the caudal tip of the splenium of the corpus callosum (right red ROI). This ROI excludes fibers from the fornix and the posterior aspect of the cingulum.

The previous result can be segmented further into three distinct areas of the corpus callosum, the anterior part or genu, the central part or body, and the posterior aspect or splenium. To achieve this segmentation, the first tracking result is taken and three new ROIs are drawn (Fig. 12.29a). The red ROI delineates the midsagittal aspect of the genu, the yellow ROI the body, and the green ROI the splenium. In Fig. 12.29b, the results

from this fiber tracking are shown in corresponding colors.

The Cingulum

The cingulum is a paired parasagittal structure that extends from the septal area to the uncus region of the temporal lobe. Due to its close proximity to the corpus callosum, especially while in proximity of the cingulate gyrus, callosal fibers are invariably included in the starting ROI. The ROI outlined in white includes the left and right cingulum. The appropriate coronal plane is found when the large green structure above the corpus callosum is selected in the sagittal plane (Fig. 12.30a). The callosal fibers can be easily removed by using the midsagittal ROI previously used as starting ROI for tracking of the corpus callosum. The final result is in Fig. 12.30b.

The Fornix

Fiber tracking of the fornix is quite challenging. First, it is a very thin structure with a relatively low fractional anisotropy, most probably due to substantial partial volume effects of the surrounding gray matter and cerebrospinal fluid. This low anisotropy may cause fiber tracking to

Fig. 12.29 Tracking of the Corpus callosum, second step. (**a**) Midsagittal view of the CC with the initial starting ROI in *white* and the sub-segmentation in *red*, *yellow*, and *green*. (**b**) Tracking result in colors corresponding to the initial ROIs
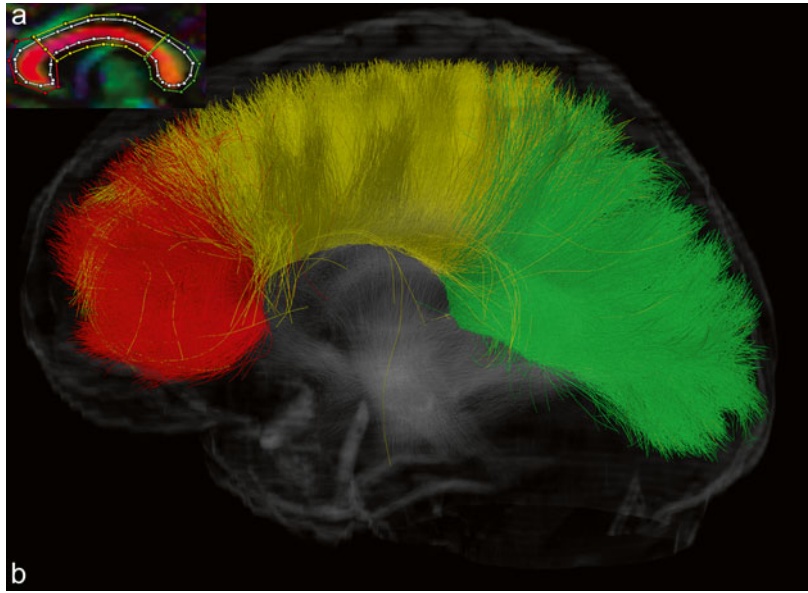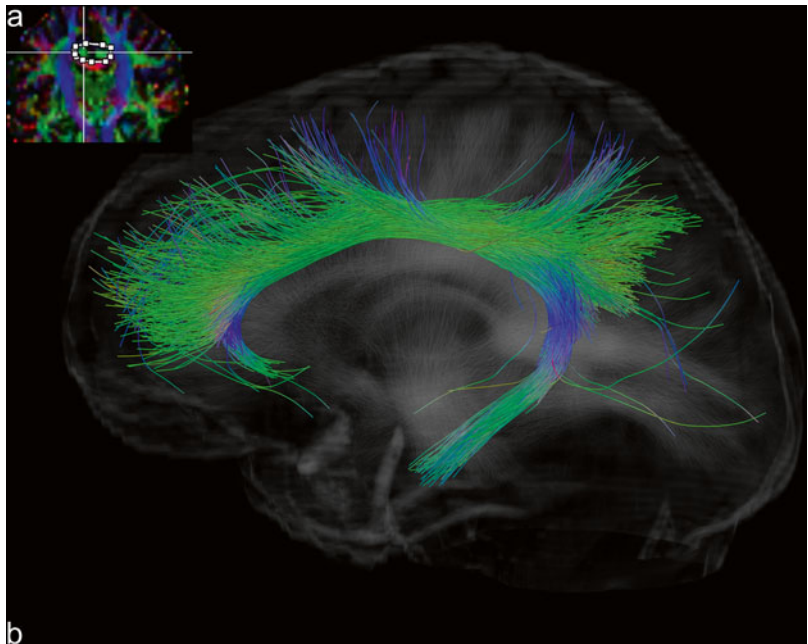

Fig. 12.30 Tracking of the bilateral cingulum bundle (CB). (**a**) Initial ROI encompassing the CB bilaterally (*white*) in the coronal plane. (**b**) Tracking result overlaid on a sagittal fiber density map

be aborted. Second, it is a highly curved structure that poses additional difficulties for fiber tracking algorithms. And finally, the fornix lies in close proximity to other fiber bundles such as the corpus callosum and the anterior commissure that further hamper fiber reconstruction. The fornix is of great interest, especially in psychiatric research on Alzheimer's, since it is one of the major tracts related to the hippocampus and memory function. Its fibers run along the medial aspect of the hippocampus, forming the fimbria, that project posterosuperiorly. The bilateral fibria form the crus, run over the thalamus, and then join to form the body. Running frontally, the corpus separates again to form the column and the majority of the fibers terminate in the mammil-

Fig. 12.31 Unilateral tracking of the fornix (FX). (**a**) Initial ROI (*white circle*) encompassing the FX in the coronal plane. (**b**) Tracking result overlaid on a sagittal fiber density map
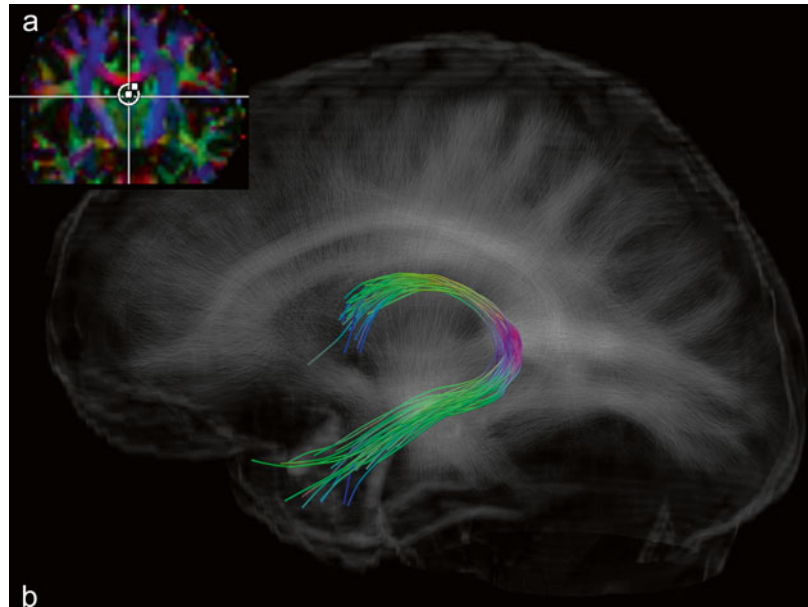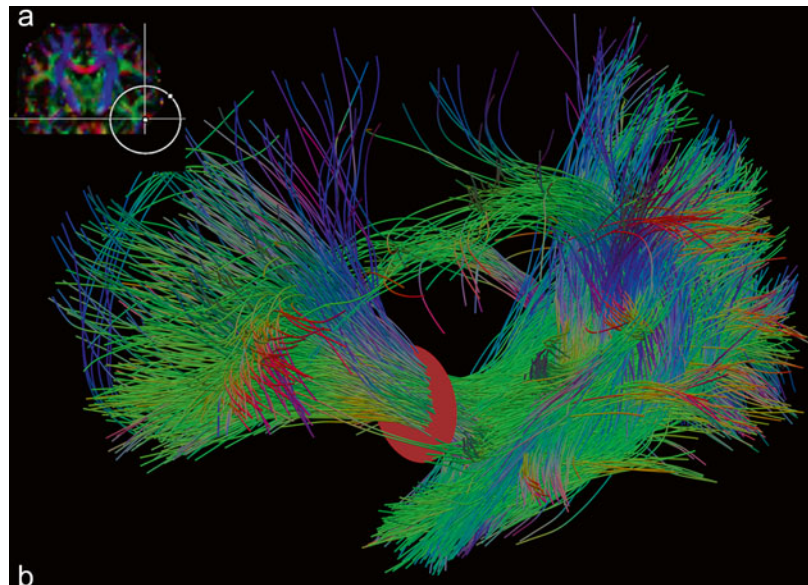

Fig. 12.32 (**a**) Initial ROI (*white circle*) for all the following tracts. (**b**) Through the red exclusion ROI, the Uncinate Fasciculus (UF) is excluded

lary body. The body of the fornix is a good starting region best found in the midsagittal plane. Then, the full fornix can be delineated on the corresponding coronal slice (Fig. 12.31a). The initial result contains spurious fibers from the corpus callosum and the anterior commissure that can be removed subsequently. The final result as shown in Fig. 12.31b is somewhat fragile and, depending on your data, may look less well defined.

The Inferior Longitudinal-, Inferior Fronto-Occipital- and Uncinate Fasciculus

Fiber tracking of the inferior longitudinal fasciculus can be started from the temporal lobe. As indicated in Fig. 12.32a, a large, somewhat nonspecific starting region can be chosen to encompass the temporal lobe on the coronal slice (right). This yields a large complex of fiber bundles (Fig. 12.32b) that can be further dissected.

Fig. 12.33 Tracking of the inferior longitudinal fasciculus (ILF). (**a**) Placement of large occipital inclusion ROI (*white circle*). (**b**) Depiction of the ILF overlaid on a fiber density map
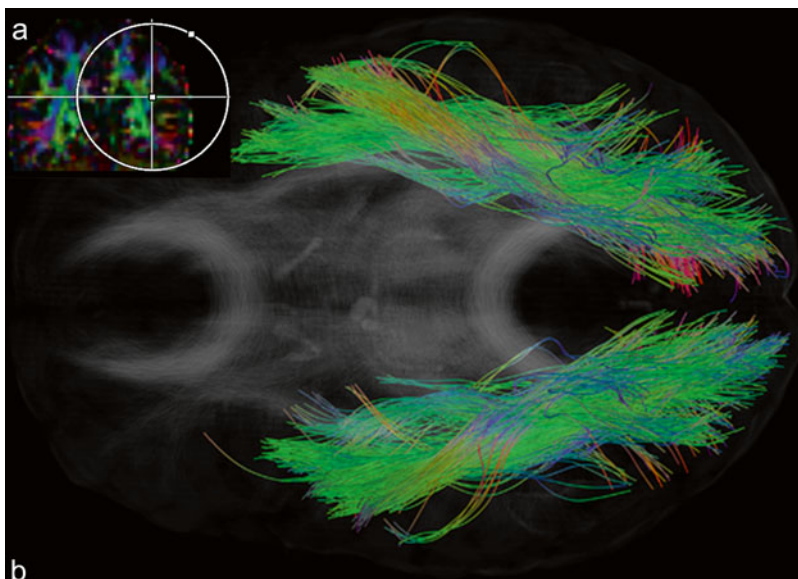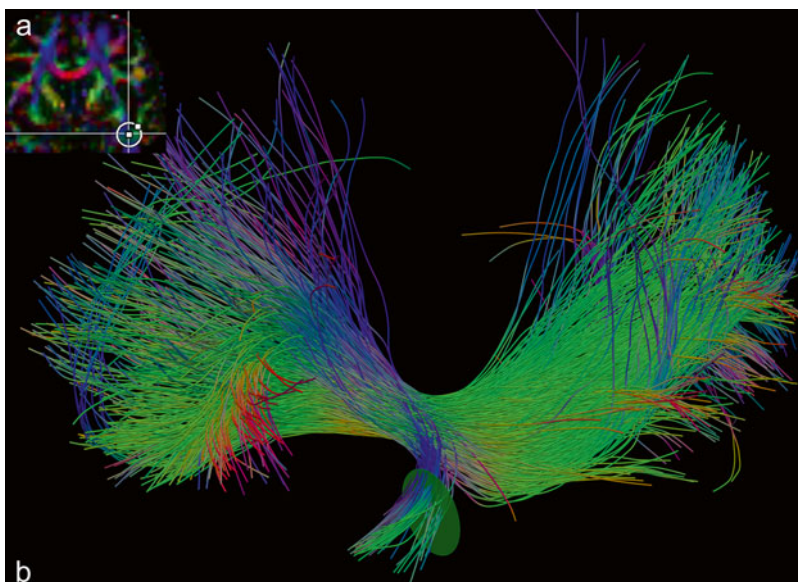

Fig. 12.34 Tracking of the uncinate fasciculus (UF). (**a**) Starting ROI at the fronto-temporal junction. (**b**) Initial tracking result and green inclusion ROI

The inferior longitudinal fasciculus is the main bundle connecting the temporal and occipital lobes. The two other major fiber bundles that are part of the initial complex (Fig. 12.32b) are the uncinate- and the inferior fronto-occipital fasciculus. These two bundles can be easily excluded by the exclusion ROI (red) indicated in Fig. 12.32b at the fronto-temporal junction. This is also a perfect starting ROI for these two structures. This is described in the next section on these two struc-

tures. Additional spurious fibers, mainly stemming from the anterior commissure and the corpus callosum, can be excluded by a large parieto-occipital inclusion ROI (Fig. 12.33a). Figure 12.33b shows the inferior longitudinal fasciculus bilaterally.

As mentioned in the previous section on the inferior longitudinal fasciculus, a coronal ROI at the fronto-temporal junction (Fig. 12.32b) is the ideal starting region for the reconstruction of the inferior fronto-occipital and uncinate fas-

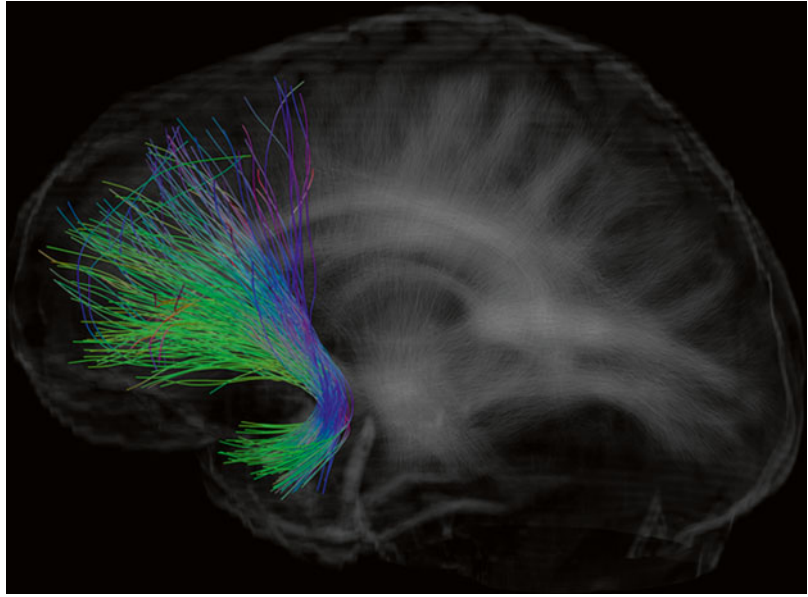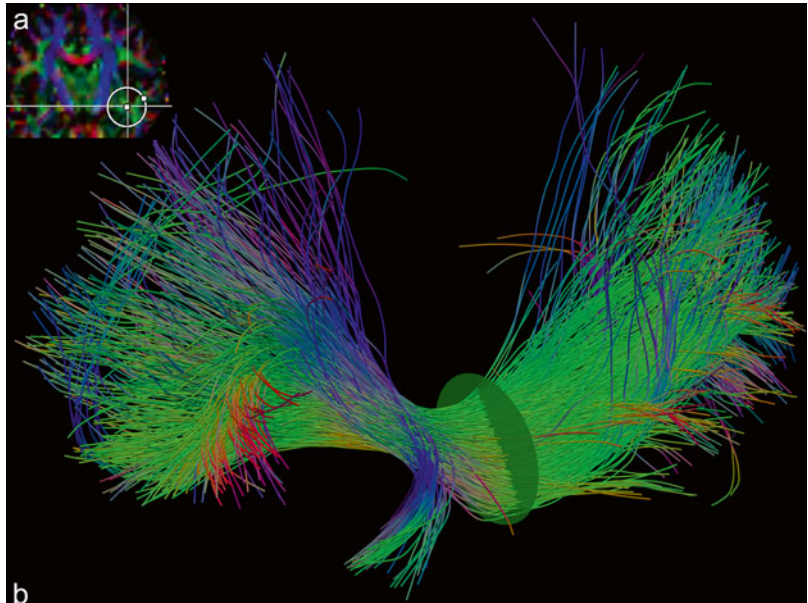**Fig. 12.35** Depiction of the UF overlaid on a sagittal fiber density map

Fig. 12.36 Tracking of the inferior fronto-occipital fasciculus (IFOF). (**a**) Initial ROI as in Fig. 12.34. (**b**) Initial tracking result and green inclusion ROI

ciculus. As can be seen in the initial result in Fig. 12.34b, no spurious fibers are present, and in two easy steps the two bundles can be isolated. To better appreciate the intricate interwoven structure of the above named three fiber bundles, this section is concluded with a combined overview. Since the uncinate fasciculus connects the frontal and temporal lobe whereas the inferior fronto-occipital fasciculus connects the frontal and occipital lobe, a second inclusion ROI, as depicted in Fig. 12.34a, b (green ROI) within the temporal lobe, effectively isolates the uncinate fasciculus. The results can be seen in Fig. 12.35. Note that no additional ROIs are required to remove spurious fibers. Likewise, the inferior fronto-occipital fasciculus can be isolated by placing an inclusion ROI directly posterior to the point where both bundles join

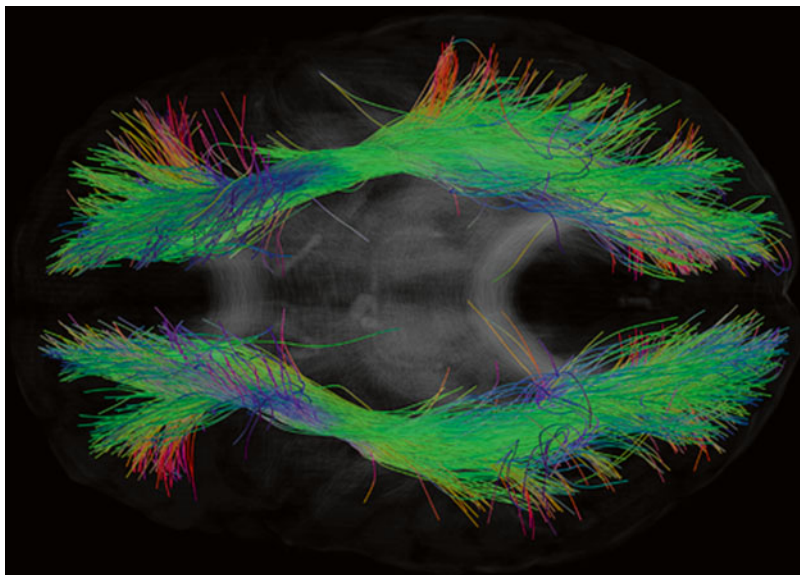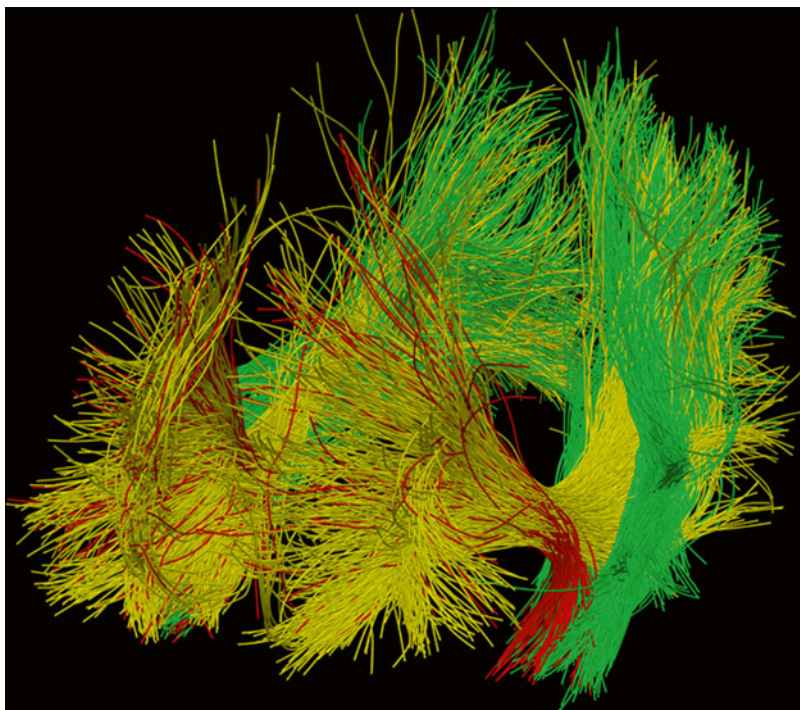**Fig. 12.37** Depiction of the IFOF overlaid on an axial fiber density map

Fig. 12.38 Combined bilateral view of the UF (*red*), the IFOF (*yellow*), and the ILF (*green*)

(Fig. 12.36a, b) and the final result is shown in Fig. 12.37.

Figure 12.38 is an overview where the previously reconstructed tracts are shown in a combined array. The uncinate fasciculus is colored red, the inferior longitudinal fasciculus is colored green, and the inferior fronto-occipital fasciculus is colored yellow.

The Superior Longitudinal-, Superior Fronto-Occipital- and Arcuate Fasciculus

The superior longitudinal, superior fronto-occipital and arcuate fasciculus can all be isolated from one starting ROI (Fig. 12.39a). The arcuate fasciculus especially is of great interest in neuroscience and neurosurgery alike, since it

Fig. 12.39 Initial ROI including the superior longitudinal fasciculus (SLF), the arcuate fasciculus (AF), and the superior fronto-occipital fasciculus (SFOF). (**a**) Initial unilateral ROI placement. (**b**) Removal of spurious fibers from the internal capsule (*white ROI*). (**c**) 3D overview of the initial tracking result and the exclusion ROI as in (**b**) (*red circle*)
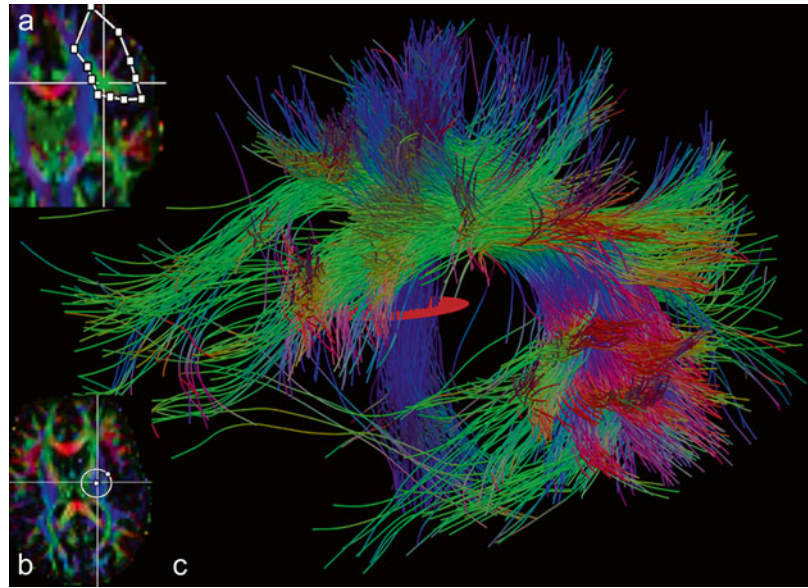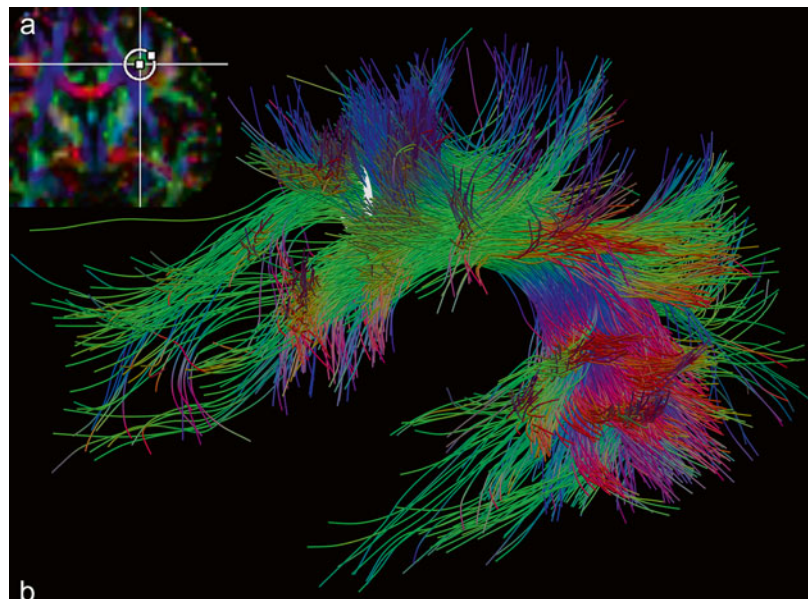

Fig. 12.40 Selection of the SFOF. (**a**) Initial ROI displayed on the coronal color map. (**b**) Depiction of the same inclusion ROI (*white circle*) on the 3D tracking result after removal of the fibers from the internal capsule

connects the speech areas of Broca and Wernicke in the dominant (mostly left) hemisphere.

Spurious fibers from the uncinate and inferior fronto-occipital fasciculus can be removed by using the starting ROI for these two bundles, as described in the previous section, as exclusion ROI. Spurious fibers from the cortico-spinal tract can be removed by placing a large ROI in the posterior limb of the internal capsule (Fig. 12.39b). The final result shown in Fig. 12.39c can be used

as a starting point to isolate the individual fiber bundles.

The superior fronto-occipital fasciculus runs slightly more medial and superiorly of the superior longitudinal fasciculus. Thus, by choosing the bundle that follows this course from the initial result, the superior fronto-occipital fasciculus can be isolated. A ROI drawn on a coronal section ensures the complete inclusion of the tract (Fig. 12.40a, b) and the result is shown in Fig. 12.41.

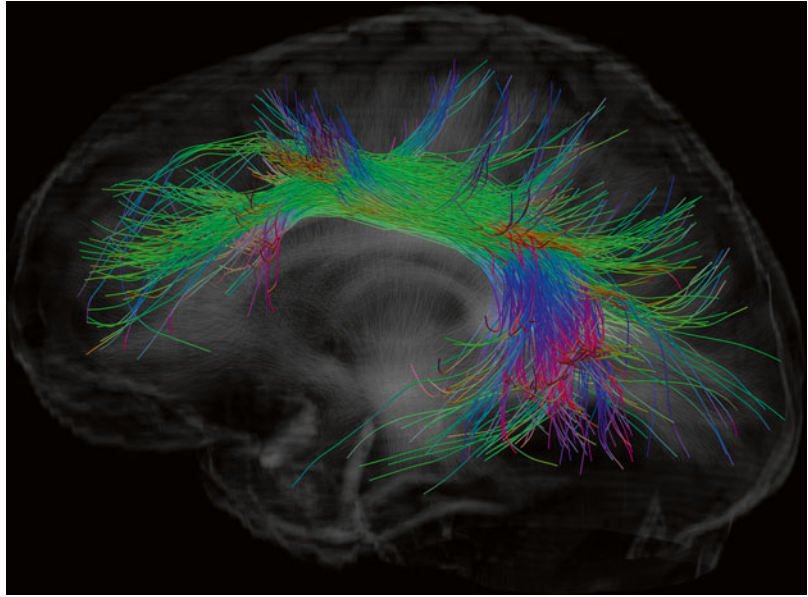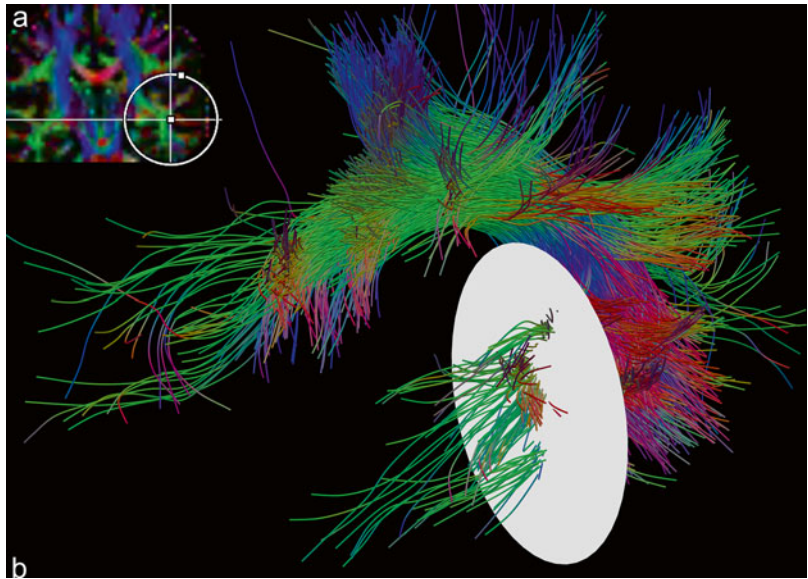**Fig. 12.41** Depiction of the SFOF overlaid on a sagittal fiber density map

Fig. 12.42 Selection of the AF. (**a**) Initial ROI displayed on the coronal color map. (**b**) Depiction of the same inclusion ROI (*white circle*) on the 3D tracking result after removal of the fibers from the SFOF

After isolation and exclusion of the superior fronto-occipital fasciculus, the result shown in Fig. 12.42b includes the arcuate and superior longitudinal fasciculus. Since the arcuate fasciculus is the only bundle of the two entering the temporal plane, a ROI placed to include this region (Fig. 12.42a, b) will effectively isolate the arcuate fasciculus. The results of this dissection are displayed in Fig. 12.43. The superior longitudinal fas-

ciculus can be obtained by excluding both the arcuate and the superior fronto-occipital fasciculus from the initial result and it is displayed in Fig. 12.44.

In Fig. 12.45, the previously reconstructed tracts are shown in a combined array. The superior fronto-occipital fasciculus is colored red, the arcuate fasciculus is colored green, and the superior longitudinal fasciculus is colored yellow.

Fig. 12.43 Depiction of the AF overlaid on a sagittal fiber density map
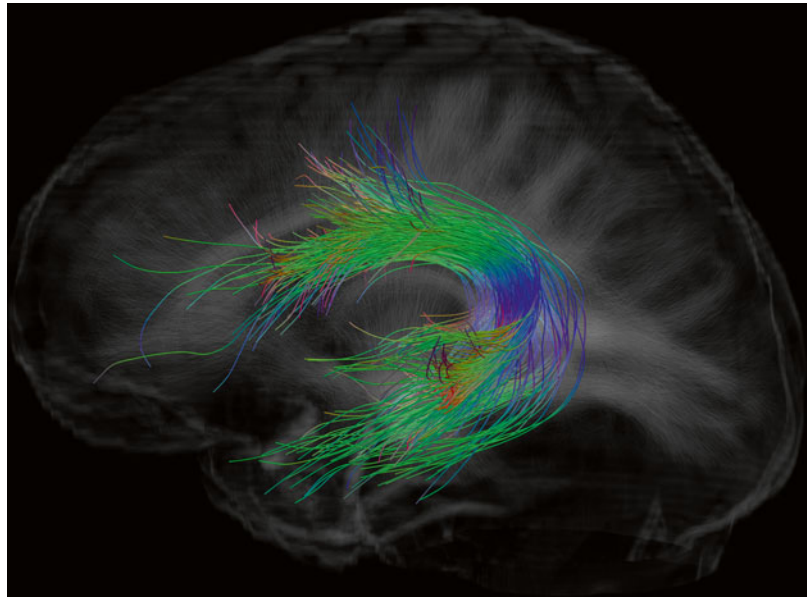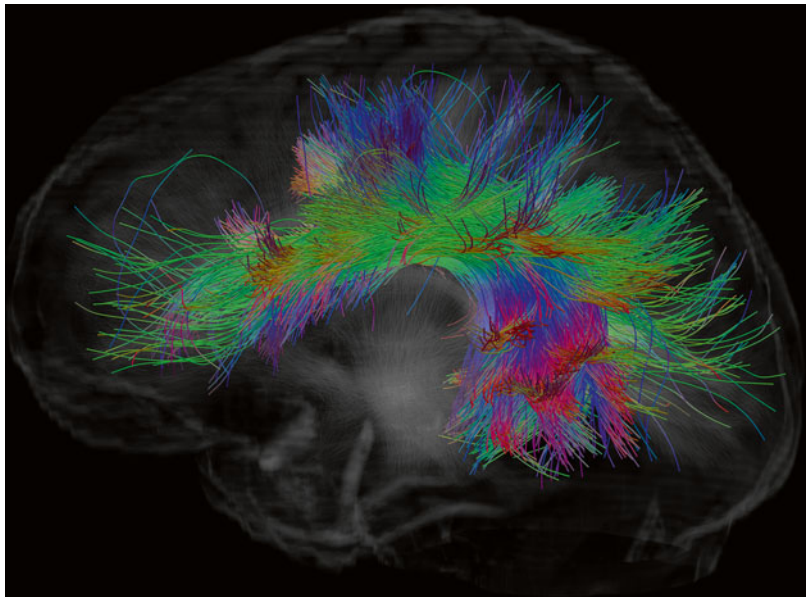

Fig. 12.44 Depiction of the SLF overlaid on a sagittal fiber density map. This image was obtained by removing the AF and the SFOF from the initial tracking result

The Cerebral Peduncles

The cerebral peduncles contain three major fiber bundles, the fronto-pontine, the cortico-spinal, and the temporo-parieto-occipito-pontine tract. The most renowned of the three is the cortico-spinal tract, as it is the main connection from the motor cortex to the spinal cord and of critical importance for motor function in humans. The initial result as shown below can be obtained by encompassing the cerebral peduncle on an axial slice as indicated in Fig. 12.46a. The initial result (Fig. 12.46b) includes all three tracts.

The fronto-pontine tract can be selected by placing a relatively large ROI in the frontal lobe.

Fig. 12.45 Combined unilateral view of the SFOF (*red*), the SLF (*yellow*), and the AF (*green*)
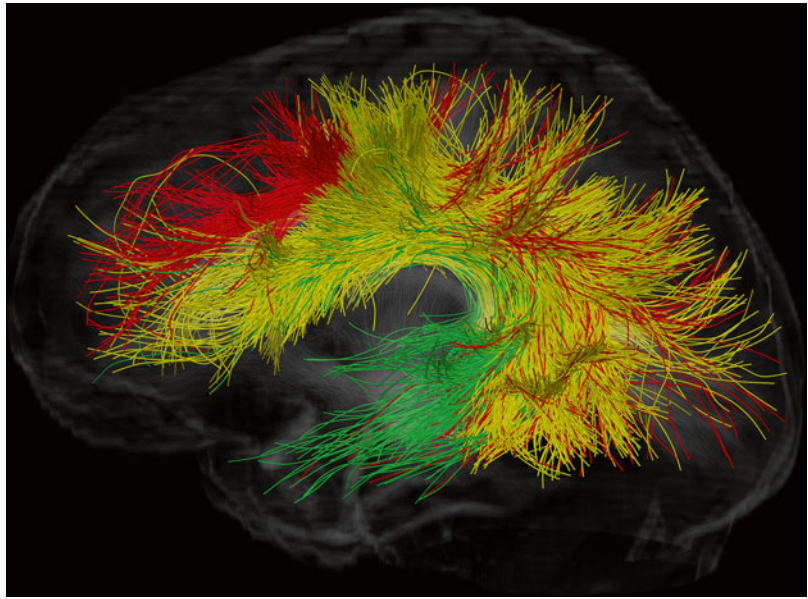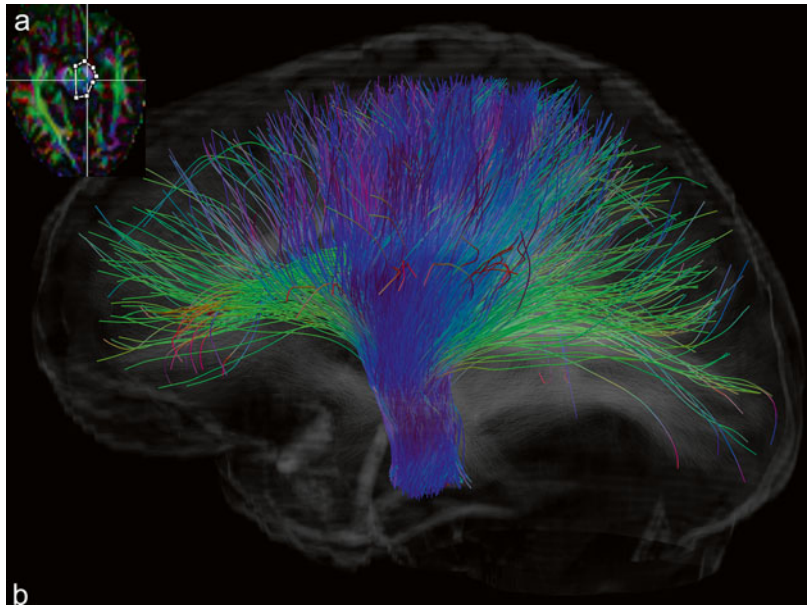

Fig. 12.46 Initial tracking of the fronto-pontine-, the cortico-spinal-, and the parieto-occipito-pontine tract (FPT, CST, and POPT respectively). (**a**) Initial ROI overlaid on an axial color map. (**b**) Initial tracking result with a combined representation of the FPT, the CST, and the POPT overlaid on a sagittal fiber density map

To include all tracts, the coronal plane should be used. The cortico-spinal tract can be selected by placing a relatively large ROI to encompass the corona radiata. To include all tracts, the axial plane should be used. The temporo-parieto-occipito-pontine tract can be selected by placing a relatively large ROI in the parieto-occipital area. To include all tracts, the coronal plane should be used. In the overview, the previously reconstructed tracts are shown in a combined array (Fig. 12.47). The fronto-pontine tract is colored red, the temporo-parieto-occipital-pontine tract is colored green, and the cortico-spinal tract is colored yellow.

Fig. 12.47 Combined unilateral view of the FPT (*red*), the CST (*yellow*), and the POPT (*green*)
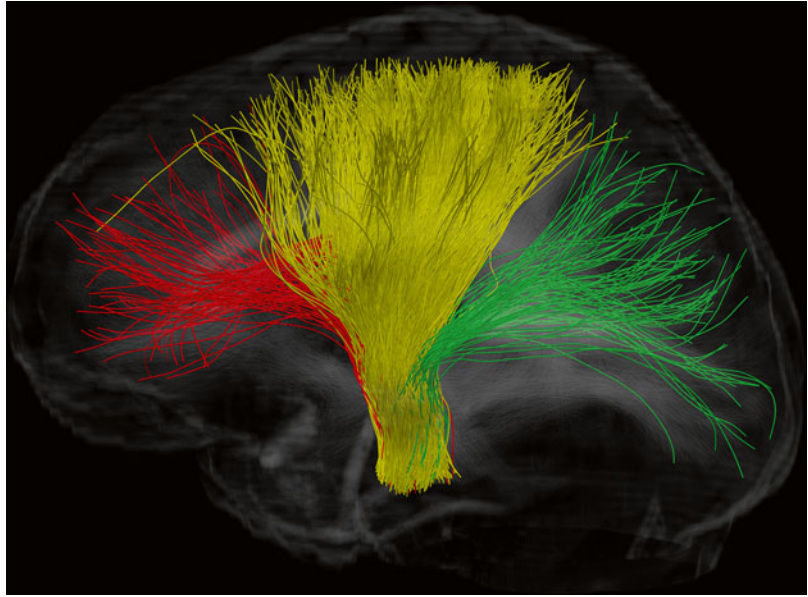
References

1. Mori S, van Zijl PC. Fiber tracking: principles and strategies - a technical review. NMR Biomed. 2002;15(7-8):468–80.
2. Mori S, Kaufmann WE, Davatzikos C, Stieltjes B, Amodei L, Fredericksen K, Pearlson GD, Melhem ER, Solaiyappan M, Raymond GV, Moser HW, van Zijl PC. Imaging cortical association tracts in the human brain using diffusion-tensor-based axonal tracking. Magn Reson Med. 2002;47(2):215–23.
3. Stieltjes B, Kaufmann WE, van Zijl PC, Fredericksen K, Pearlson GD, Solaiyappan M, Mori S. Diffusion tensor imaging and axonal tracking in the human brainstem. NeuroImage. 2001;14(3):723–35.
4. Xue R, van Zijl PC, Crain BJ, Solaiyappan M, Mori S. In vivo three-dimensional reconstruction of rat brain axonal projections by diffusion tensor imaging. Magn Reson Med. 1999;42(6):1123–7.
5. Mori S, Crain BJ, Chacko VP, van Zijl PC. Three-dimensional tracking of axonal projections in the brain by magnetic resonance imaging. Ann Neurol. 1999;45(2):265–9.
6. Hahn HK, Klein J, Nimsky C, Rexilius J, Peitgen HO. Uncertainty in diffusion tensor based fibre tracking. Acta Neurochir Suppl. 2006;98:33–41.
7. Conturo TE, Lori NF, Cull TS, Akbudak E, Snyder AZ, Shimony JS, McKinstry RC, Burton H, Raichle ME. Tracking neuronal fiber pathways in the living human brain. Proc Natl Acad Sci U S A. 1999;96(18):10422–7.
8. Reisert M, Mader I, Anastasopoulos C, Weigel M, Schnell S, Kiselev V. Global fiber reconstruction becomes practical. NeuroImage. 2011;54(2):955–62.
9. Kreher BW, Mader I, Kiselev VG. Gibbs tracking: a novel approach for the reconstruction of neuronal pathways. Magn Reson Med. 2008;60(4):953–63.
10. Mangin JF, Poupon C, Cointepas Y, Riviere D, Papadopoulos-Orfanos D, Clark CA, Regis J, Le Bihan D. A framework based on spin glass models for the inference of anatomical connectivity from diffusion-weighted MR data - a technical review. NMR Biomed. 2002;15(7-8):481–92.
11. Fillard P, Descoteaux M, Goh A, Gouttard S, Jeurissen B, Malcolm J, Ramirez-Manzanares A, Reisert M, Sakaie K, Tensaouti F, Yo T, Mangin JF, Poupon C. Quantitative evaluation of 10 tractography algorithms on a realistic diffusion MR phantom. NeuroImage. 2011;56(1):220–34.

MITK Diffusion Imaging

12. Fritzsche KH, Neher PF, Reicht I, van Bruggen T, Goch C, Reisert M, Nolden M, Zelzer S, Meinzer HP, Stieltjes B. MITK Diffusion Imaging. Methods Inf Med. 2012;51(5):441–8.

13. Stieltjes B, Brunner R, Fritzsche KH, Laun FB. Diffusion tensor imaging; introduction and atlas. Heidelberg: Springer; 2012.

Suggested Reading

Nieuwenhuys R, Voogd J, Van Huijzen C. The human central nervous system; a synopsis and atlas. New York: Springer; 1988. A great anatomical work of reference for brain anatomy.

Johansen-Berg H, Behrens TEJ. Diffusion MRI; from quantitative measurement to in vivo neuroanatomy. Amsterdam: Academic; 2009. Chapters 5-7 give a great overview of the relationship between microstructure and DTI-derived parameters.

Stieltjes B, Brunner R, Fritzsche KH, Laun FB. Diffusion tensor imaging; introduction and atlas. New York: Springer; 2012. Gives a more detailed introduction to diffusion imaging and rich anatomical reference.